PHYTOPLANKTON RESPONSES TO SHIFTING IRON-TEMPERATURE CONDITIONS IN THE IRMGINGER BASIN

By

Lena Beckley

Submitted in partial fulfilment of the requirements

for the degree of Masters of Science

at

Dalhousie University

Halifax, Nova Scotia

August 2023

Table of Contents

List of Tables

List of Figures

Abstract

The High Latitude North Atlantic is a globally significant region of deepwater formation home to intense primary productivity. Controls on phytoplankton growth in this region remain poorly constrained but are thought to seasonally be dominated by iron availability, with the potential to be influenced by predicted increases in sea surface temperatures. We conducted iron-temperature experiments in the Irminger Basin in late summer of 2021 to examine the impact of iron addition, with and without changes in temperature, on phytoplankton. We found clear evidence of iron limitation and that iron and temperature interactively impacted phytoplankton growth. Bacillariophyta responded to iron addition, and metaproteomic analyses revealed diverging strategies between Bacillariophyta and Prymnesiophyceae to iron-limiting conditions. Bacillariophyta deployed photosynthesis-related protein responses to manage iron stress regardless of changes in temperature. These interactive iron-temperature effects on phytoplankton growth have implications for the future of bloom progression and the biogeochemistry in this key marine region.

List of Abbreviations and Symbols Used

ASV: Amplicon Sequencing Variant

Chl-a: Chlorophyll a

DNA: deoxyribonucleic acid

DTT: dithiothreitol

FA: formic acid

HLNA- High Latitude North Atlantic

HPLC: High-performance liquid chromatography

MG-MetalGate

MS: mass spectrometer

PAR: Photosynthetically active radiation

PCR: polymerase chain reaction

POC: particulate organic carbon

QIIME: quantitative insights into microbial ecology

RNA: ribonucleic acid

RV: research vessel

SDS: sodium dodecyl sulfate

SST: sea surface temperature

TEAB: triethylammonium bicarbonate

Acknowledgements

I would like to thank my supervisor, Erin Bertrand for her unwavering guidance and support along this project. I would also like to thank my committee members, Rob Middag and Julie LaRoche for their insights and suggestions. I would particularly like to thank Rob Middag for his role as Chief Scientist on the MetalGate cruise, and for creating an effective, positive, and collaborative working environment at sea. To all members of the Bertrand Lab I would like to say it has been an extreme privilege to work together and learn from each other. I would like to thank both Loay Jabre and Elden Rowland for their several contributions to this project, but also for the inspiring and thought-provoking conversations and perspectives along the way. To all the countless family and friends who have supported me in this endeavor, your support has meant so much. To my Grandfather, Marshall Wiebe, I would like say thank you for constantly inspiring me to research and appreciate the natural environment, from rivers to seas.

Chapter 1: Introduction

1.1 The High Latitude North Atlantic biogeochemical importance

Oceanographic dynamics in the High Latitude North Atlantic (HLNA), including the Nordic Seas, are extremely complex. It is in this region that Arctic and Atlantic water masses converge. Thus, the Nordic Seas serve as a gateway between distinct water bodies and form a biogeochemical nexus (Logemann et al., 2013; Rudels et al., 2005). The HLNA also is also home to productive spring phytoplankton blooms (Moore et al., 2005; Sanders et al., 2005). Phytoplankton require light, macronutrients and trace nutrients for growth. Much of the year can be light limiting for phytoplankton in the HLNA, however, springtime results in increased light availability through the shallowing of the mixed depth layer and longer daylight hours. Nutrients are delivered to the surface ocean from deep waters via winter convective mixing and come springtime, phytoplankton harness both light and nutrients to create large blooms and draw down nutrient concentrations (Sverdrup, 1953). Some of this biomass sinks out of the photic zone, and contributes to carbon export, a process referred to as the biological carbon pump (Eppley & Peterson, 1979). As the headwaters for deep water formation that drives thermohaline circulation, this region has far-reaching impacts (Dickson et al., 2008). Indeed, the HLNA has one of the longest-term storage capacities from the biological pump, where the fraction of phytoplankton biomass that makes it to depth may be sequestered in the deep ocean for up to a millennium (DeVries et al., 2012). Leftover nutrients at the onset of deep-water formation (preformed nutrients) are another key biologically mediated feature with far-reaching impacts (Marinov et al., 2008). Excess nutrients present at the onset of deep-water formation have the potential to alter downstream productivity dynamics once upwelled, thus changes to productivity and nutrient use in the HLNA are consequential to other regions.

1.2 Iron limitation in the High Latitude North Atlantic

Leftover macronutrients have been observed in the HLNA in the summer months, after the spring bloom has subsided, indicating that some other factor limits growth and results in an inefficiency in the biological carbon pump (Cullen, 1991). Mounting evidence suggests Fe may seasonally limit growth in certain areas of the HLNA,

particularly the Irminger and Iceland Basins (Achterberg et al., 2018; Measures et al., 2008; Nielsdóttir et al. 2009). Late-summer Fe concentrations in the HLNA have been consistently reported to be sub 0.1 nM (Achterberg et al., 2018; Measures et al., 2008; Nielsdóttir et al., 2009).

To date, literature on iron limitation in the HLNA is complex, indicating high interannual and regional (inter-basin) variability. In the Irminger Basin excess surface nitrate, between 2-6 μM, has been observed in the summer months (Achterberg et al., 2018; Ryan-Keogh et al., 2013; Sanders et al., 2005). Leftover surface nitrate has also been reported in the Iceland Basin in the summer months (Nielsdóttir et al., 2009; van de Poll et al., 2013). However, complete drawdown of surface nitrate was observed in this Basin in the summer of 2010 (Achterberg et al., 2018; Ryan-Keogh et al., 2013). In Spring of 2010, a volcanic eruption (Eyjafjallajökull) in Iceland resulted in highly concentrated fine-scale ash deposition in the Iceland Basin and has been proposed to have contributed to complete nitrate drawdown in the Iceland Basin summer of 2010 (Achterberg et al., 2013). Anomalously high surface dFe concentrations were observed in the Irminger Basin in early summer of 2014, which could have been due to bloom progression dynamics, or perhaps driven by deeper winter mixing (Tonnard et al., 2020). It appears that this region is on the precipice of varying degrees of seasonal iron limitation, which may be highly responsive to changes to inputs, as well as shifting oceanographic dynamics.

1.3 Projected changes to HLNA waters

At a first order the potential amount of carbon export from bloom biomass is contingent on the initial dissolved nutrients and their ratios, as well as the community which responds to those nutrients. Shifting sea surface temperatures (SST) may impact both conditions in the HLNA. SST increases are projected for the seas surrounding Iceland, with more pronounced warming anticipated north of Iceland and during late-summer months (Alexander et al., 2018). For instance, SST is projected to increase by as much as ~0.5°C per decade (1976–2099) in both the Iceland and Norwegian Seas during late-summer months based on model simulations from the National Center for

Atmospheric Research Large Ensemble Community Project (CESM-LENS) (Alexander et al., 2018).

Temperature and salinity are two factors which govern density, and therefore stratification dynamics. Increased stratification is anticipated in the HLNA, which may impact nutrient supply to the photic zone (Capotondi et al., 2012). Shallower winter mixing affects not only macronutrient re-supply to surface waters (such as nitrogen and phosphorous), but also micronutrients such as Fe. Winter convective mixing is thought to be the largest source of dissolved Fe to surface waters in the HLNA, as aeolian transport is limited (Achterberg et al., 2018). Temperature is widely known to be a dominant factor in constraining phytoplankton distributions (Acevedo-Trejos et al., 2013). Increasing temperatures in conjunction with shifting current dynamics can provide the opportunity for northward range-expansion and shifts in community composition (Oziel et al., 2020). Recent work has also shown temperature to be a distinctly influential factor in phytoplankton communities surrounding Iceland, with clear delineations of groups in either Atlantic or Arctic water masses (Cerfonteyn et al., 2023). This is consequential as carbon export efficiency has been shown to be highly dependent on community composition, with species such as diatoms dominating expected export efficiency (Boyd, 2010). It has also been proposed that increased temperatures may drive shorter bloom periods, whereby nutrients are exhausted earlier in the season, thus shifting the temporal dynamics of primary productivity. This may have cascading impacts as phytoplankton form the base of the marine food chain, and disjointed relationships between life cycles and bloom periods could impact higher trophic levels (Rose et al., 2009). With anticipated changes to temperatures and iron delivery to the HLNA, it is imperative to examine both the individual and interactive effects of these variables on primary producers of this region. Downstream consequences may be far-reaching, influencing biological carbon storage, trophic-interactions and the composition of preformed nutrients.

1.3 Fe-Temperature effects on phytoplankton

There are several phytoplankton cellular requirements for Fe, the largest of which is in the photosynthetic electron transport chain. Fe is also required for nitrate

assimilation, and in superoxide dismutases (Raven, 1988; Raven et al., 1999). Fe requirements in the photosynthetic electron transport chain stem from Fe in PS II (2-3 Fe), PS I (12 Fe), cytochrome *b6-f* (5 Fe) and ferredoxin (2 Fe) (Raven et al., 1999). Fe is required in nitrate assimilation, in the enzymes nitrate and nitrite reductase (Raven, 1988). Being critical in energy and nutrient acquisition, Fe is a key regulator of phytoplankton growth in the global oceans (Moore et al., 2013).

Fe and temperature effects on phytoplankton have individually been extensively studied (Schoffman et al., 2016). However, there remains much to learn about the interactive nature of how these two variables impact phytoplankton growth. Fe and temperature may have compounding effects as there is a distinct decoupling of temperature effects in phytoplankton growth, where temperature influences enzymatically catalyzed reactions, while not exerting influence on photochemical reactions, which critically includes the primary photochemical reactions of photosynthesis (Raven & Geider, 1988). Here lies the capacity for Fe and temperature effects to be highly interactive, as Fe availability does have the capacity to affect the light component of photosynthesis, due to the high molecular Fe cost associated with both photosystems (Raven et al., 1999).

Studies examining interactive effects of temperature and iron on phytoplankton have been conducted *in situ* in the Southern Ocean, as well as in culture experiments. Several studies have found interactive effects of temperature and Fe influencing phytoplankton growth (Andrew et al., 2019; Rose et al., 2009; Jabre et al., 2021, Jabre et al., 2020). Fe sufficiency has been shown to increase upper thermal tolerance in several Southern Ocean species (Andrew et al., 2019). Fe-temperature effects have been shown to strongly influence nutrient uptake, with Fe addition experiments demonstrating increased nutrient uptake rates at higher temperatures (Rose et al., 2009; Spackeen et al., 2018). This previous Southern Ocean work demonstrates that temperature and Fe can have interactive effects on the growth of High Latitude phytoplankton species. The HLNA remains less studied with respect to Fe limitation, and essentially unstudied in terms of interactive effects of Fe and temperature.

There has been a recent awareness of the need for multiple-stressor studies (Boyd et al., 2010, 2015). Importance has been placed on co-limiting relationships with nutrients and light (Saito et al., 2008; Schoffman et al., 2016). It is also imperative to understand how these relationships are impacted in conjunction with environmental factors such as temperature change (Boyd et al., 2010). This is necessary to obtain a more comprehensive understanding of how climate change will influence primary producers, with projected nutrient and temperature changes. Furthermore, although single-species culture studies are mechanistically informative, it is also critical to understand whole community responses. Incubation experiments of the natural phytoplankton community (termed bioassay experiments) have long been deployed in the field to assess community response to environmental variables, be it nutrient additions, or changes to light levels or temperature. These experiments typically involve collection of surface sea water, manipulations to variables of interest, and tracking of community responses over relevant timescales, usually from hours to weeks (Beardall et al., 2001).

1.5 Metaproteomic approaches: bridging the gap

Classical methods of interrogating physiological impacts of nutrient stress of phytoplankton communities *in situ* are typically limited to assessing changes in the bulk community, or at a finer grain a size-fractioned proportion of the community. Depending on the community composition, bulk measurements can be more or less informative of species-specific responses to manipulations. Culture experiments are often used to validate *in situ* observations; however, culture experiments do not capture a fully representative 'wild' community response, with community-scale interactions. Recent advances in metaproteomics offer a potential bridging of this gap (McCain et al., 2022). Metaproteomics is defined as a snapshot of proteins expressed in a microbiome at a given timepoint (Wilmes & Bond, 2004). A typical metaproteomics workflow is achieved through extraction of protein from environmental samples, this extract is then digested into peptides and analyzed via mass spectrometry. Here, peptide-derived mass spectra are obtained and matched to potential peptide sequences through database searching, where the identified peptides also receive both functional and taxonomic assignments (Saito et al., 2019). This information allows for the investigation of realized cellular protein

allocation patterns and investment strategies of different community members within a natural matrix (McCain et al., 2022).

Recent work has leveraged functional annotations to determine the proteomic investments in different coarse-grained functional pools. This approach broadly looks at a pool of peptides assigned a given function, for instance all peptides identified as contributing to ribosomes. The sum of these peptide abundances normalized to the total peptide abundances in a sample would constitute the proteomic allocation to ribosomes and by extension the proteomic investment in a critical cellular function-protein synthesis. This calculation can be conducted for different functional pools and taxonomic groups, where the summed peptides for a functional pool from a particular taxonomic group is normalized to the total peptide abundance of that group. This has been termed a 'proteomic mass fraction' and allows for functional proteomic allocation strategies to be elucidated from specific groups within complex communities (McCain et al., 2022). Conducting proteomic data analysis with these coarse-grained approaches, both functionally and taxonomically, minimizes biases such as co-fragmentation, and enables more robust quantitative comparisons between groups of proteins (McCain & Bertrand, 2019). We were able to leverage this approach to interrogate group-specific responses of the natural phytoplankton community to manipulated iron and temperature conditions in the HLNA.

Single-protein stress markers have been deployed since the mid-90s to interrogate iron-stress in the field (LaRoche et al., 1996). Photosynthetic-associated iron-stress indicator proteins have included flavodoxin and plastocyanin. Both these proteins serve as electron-carriers in the photosynthetic electron transport chain and can substitute for iron-containing homologs under iron-stress. However, research continues to unveil nuances in the expression patterns of these proteins in response to iron-stress and other environmental variables. For example, flavodoxin has been lost in some coastal phytoplankton species, and both iron responsive and non-iron responsive forms of flavodoxin are found in others (Toulza et al., 2012; Erdner et al., 1999; Whitney et al., 2011). Plastocyanin is not consistently iron-responsive and has been also shown to respond to temperature (Jabre et al., 2021). Despite these complexities, these proteins

remain useful diagnostics for unravelling the nutrient stress in phytoplankton, both in the field and in response to multi-stressor studies. Here we leveraged metaproteomics to interrogate expression levels of flavodoxin and plastocyanin in response to Fe-temperature manipulations and examined their expression across throughout the Irminger Basin.

To assess the status of iron limitation in the Irminger Basin we conducted a five day long shipboard incubation of the surface phytoplankton community. Iron additions were conducted at two temperatures to interrogate if there were interactive effects between iron and temperature on the community under potential future ocean-warming conditions. We then leveraged a suite of methods to examine community composition in conjunction with biogeochemical measurements. This multi-tiered approach provided an opportunity to inter-compare several compositional datatypes assessing the photosynthetic microbial community in a region which has historically been lacking characterization. Metaproteomics allowed us to interrogate group-specific protein allocation patterns and their response to iron-stress under different temperatures. We found clear signs of iron limitation in the Irminger Basin and found diatoms to be extremely responsive to iron additions, leveraging a variety of key molecular mechanisms to do so.

Chapter 2: Methods

2.1 MetalGate cruise

Samples were collected on the MetalGate research expedition 64PE474. The expedition took place on the RV Pelagia July 18th-August 16th 2021 setting sail from Reykjavik, Iceland. A total of 38 stations were sampled, 3 of which are included in this thesis, with an additional shallow station (station 4) sampled for collection of surface water for a bioassay experiment (see S1 for station coordinates).

2.2 Trace metal clean water collection

Trace metal clean sampling was conducted using an ultraclean CTD system (UCC) 'Titan' specifically constructed for trace metal clean sample collection (De Baar et al., 2008). The Titan system was mounted with 24 large volume 'Pristine' samplers each with a 23 L capacity made of Polypropylene (Rijkenberg et al., 2015). The Titan system was lowered using a Kley France winch designed for ultra-clean deployments. Once onboard the vessel the UCC was immediately transferred to a designated ultra-clean shipping container lab space for trace-metal clean sampling.

2.3 Bioassay conditions

The bioassay experiment was conducted using custom-built temperature-controlled incubators (NIOZ) mounted on the ship deck of RV Pelagia. Incubators were positioned on the front deck to minimize any light interference by shading. Two layers of neutral density screens were placed over the incubators to achieve ~15% surface irradiance conditions inside the incubation bottles.

Water collection for the bioassay was executed using the UCC system, from 25m depth at station 4. Incubations were conducted in 20 L trace-metal cleaned cubitainers, with and without 2 nM ^{57}Fe additions and kept at temperature in the tanks. Incubators were kept at two temperatures, an *in situ* temperature (9.1°C), which was the ambient temperature of surface water at the collection site, and an elevated +4°C temperature (13.1°C). Bioassay treatments included a +2nM Fe treatment, no added Fe and +4°C, +2nM Fe at *in situ* temperature, and no added Fe at *in situ* temperature. The duration of the experiment was 5 days, with a 30% dilution of all experimental treatments with fresh surface seawater after 48h, to ensure the community did not exhaust macronutrient supply over the duration of the experiment. For the dilution, filtered surface seawater,

which was collected at the same time as our initial community at $T_{0,}$ was used. 2 nM Fe was added to the diluent for the +Fe treatments. All sub-sampling of the bioassay, including T_0, T_{48} and T_f were conducted in the trace-metal clean container laboratory for trace-metal sensitive samples, with water then being allocated for other sampling methods outside designated trace-metal clean areas. The bioassay was conducted by Rob Middag, Willem van de Poll, Loay Jabre and Lena Beckley, with assistance from other members of the cruise to transport water.

2.4 Pigments

Pigments were sampled from the UCC. 3-4L of water was filtered onto 47 mm GF/F filters under mild vacuum. Samples were snap frozen in liquid nitrogen and stored at -80°C. High performance liquid chromatography (HPLC) was preformed at the University of Groningen, Netherlands. Filters were freeze dried (48 h) and pigments were extracted (48 h at 4 °C) from the filters in the dark using 90% acetone (van Leeuwe et al., 2006). High performance liquid chromatography (HPLC) pigment separation was performed using a Waters HPLC (model 2690), with cooled autosampler at (4°C) equipped with a 3.5 μm particle size Zorbax Eclipse XDB-C8 column (Van Heukelem & Thomas, 2001). Detection was based on retention time and diode array spectroscopy at 346 nm (Waters 996 HPLC Photodiode Array Detector). Pigments were quantified manually using DHI LAB standards. CHEMTAX v1.95 (Mackey et al., 1996) was used for determining taxonomic phytoplankton community composition using initial pigment ratios for diatoms, two groups of chlorophyll c3 containing algae (here called haptophytes, pelagophytes), cryptophytes, chlorophytes, *Synechococcus*, and dinoflagellates. Afterwards, pelagophytes and haptophytes were pooled. Taxonomic composition was expressed relative to chl-a. Pigment sampling was conducted by Willem van de Poll and Anna Koek.

2.5 Photosynthetic characteristics by fast repetition rate fluorometry (FRRf)

Fast repetition rate fluorometry (FRRf) measurement were conducted onboard. Water was collected from the UCC and after 30 min dark acclimation on ice, Fast Repetition Rate fluorometry (FRRf) was used to determine chlorophyll a fluorescence (chl a $_{F0}$) and maximum quantum efficiency of PSII (F_v/F_m). A volume of 3.5 mL was pipetted in the ice water cooled cuvette of the FRRf (FastOcean Sensor fitted with an

Act2 laboratory system, and Act2Run software, Chelsea Technologies Group). The instrument was used in a single turnover mode with a saturation phase of 100 flashlets on a 2 µs pitch, and a relaxation phase of 40 flashlets on a 60 µs pitch. The excitation wavelength of the FRRf's light-emitting diodes was 450 nm. Measurements in darkness were used for this manuscript (i.e., measurements without actinic light). Photophysiological measurements were conducted by Willem van de Poll and Anna Koek.

2.7 Particulate organic carbon

Particulate organic carbon (POC) was sampled at T_0 and T_f of the bioassay experiment. For each bioassay treatment, 1L of water was collected in dark bottles, and then filtered through pre-combusted 25mm glass microfiber filters (GF/G, 0.7µm) using a mild vacuum pump system (<0.2 mbar). Directly following filtration, filters were wrapped in aluminum foil and snap frozen in liquid nitrogen and then stored at -80°C. Onshore POC analysis was conducted at NIOZ using a Thermo-Interscience Flash EA1112 Series Elemental Anlayzer (Thermo Scientific) (Verardo et al., 1990). Sample collection was conducted by Willem van de Poll and Anna Koek, samples were analyzed by Willem van de Poll.

2.8 Nutrient sampling- environmental and experimental

Water for nutrient samples were obtained from the UCC in high-density polyethylene syringes (Terumo®). Samples were then transferred into 5 mL polyethylene vials. Samples that were not analyzed within 2-4h of sampling were stored in a refrigerator at 4°C. Macronutrient (phosphate, ammonium, nitrite and nitrate) measurements were conducted using a continuous gas-segmented flow QuAAtro Auto-Analyser produced by SEAL Analytical. Nutrients were measured onboard by Sharyn Ossebaar.

2.9 Trace metal sampling

Dissolved metals were filtered directly from the 'Pristine' polypropylene tubes over a 0.2 µm PEC Acropak filter under 0.5 bar inline filtered nitrogen pressure and then acidified to ~1.7 pH using ultra clean HLC (Normatom Ultrapure, VWR). Samples were then analyzed for Multi-Element (ME) determination on shore using a SeaFAST system and a High-Resolution Sector Field Inductively Coupled Plasma Mass Spectrometer (HR-

ICP-MS) (Gerringa et al., 2020). Trace metal sampling was executed by Rob Middag, Rebecca Zitoun and Patrick Laan.

2.10 Protein, RNA, DNA sampling

Protein, RNA and DNA sampling were all conducted in a temperature-controlled shipping container kept near sea surface temperatures. For protein field samples water was obtained from the UCC and sequentially filtered through 3 and 0.2 µm polycarbonate filters using a peristaltic pump. Approximate volumes filtered for proteins from field stations was ~4-10L. Once field samples were extracted, the two size-fractions were pooled prior to digestion. Proteins collected from the bioassay experiment were not size-fractioned, all the sample was filtered onto a 0.2 µm filter. RNA/DNA samples from the bioassay were also not size-fractioned, ~4L was filtered onto a 0.2 µm polycarbonate filter. Following filtration filters were placed in 2mL cryovials and stored at -80°C until extraction and analysis was conducted at Dalhousie University. Protein and DNA/RNA sampling was conducted by Lena Beckley and Loay Jabre.

2.11 Protein extraction

Protein was extracted from 0.2 and 3.0 µm polycarbonate filters. While on ice, 750 µL of 2% SDS extraction buffer (0.1 M Tris/HCl pH 7.5, 5% glycerol, 5 mM EDTA, 2% SDS) was added to each sample. After 10 minutes, the samples were heated at 95 °C while mixing at 350 RPM for 15 minutes. Next, the filters were sonicated on ice for 1 minute each using a Qsonica Sonicator (Newtown, CT). Settings for the sonicator were 50% amplitude, 125 W, pulse 15s on, 15s off. After sonication, the filters were incubated for 30 minutes at room temperature with a gentle vortex every 10-15 minutes. At this point, the supernatant was separated from the filter and transferred into a clean 2 mL centrifuge tube. The sample was centrifuged at 15 000 g for 30 minutes, with the centrifugation time increased to 45 minutes if the cell pellet was still dispersed or not well formed, which happened most often for the 3 µm filters. The supernatant was then transferred to a new 2 mL centrifuge tube (safe-lock, Eppendorf). The tube was weighed before and after the transfer of the supernatant to determine the volume of extract obtained, assuming a density of 1 mg/mL. Protein concentration was determined using a Micro BCA Protein Assay Kit (Thermo ScientificTM). Protein extraction was conducted by Lena Beckley with assistance from Elden Rowland.

2.12 Protein digestion

Between 20-60 µg of protein was digested with trypsin using S-trap mini columns (Protifi, USA). Protein extracts were reduced by adding 5 mM dithiothreitol (DTT, Sigma-Aldrich 97%) dissolved in 50 mM ammonium bicarbonate (Ambic) and incubated at 37 °C for 1 hour, 350 RPM. After cooling to room temperature, the extract was alkylated by adding 15 mM iodoacetamide (Sigma-Aldrich, BioUltra) dissolved in 50 mM Ambic. The sample was vortexed briefly, spun down, and left to incubate for 30 minutes at room temperature in the dark. Next, another 5mM DTT was added at room temperature and vortexed. Next, 12% phosphoric acid was added to obtain 1.2% concentration in the sample. S-Trap buffer (90% aqueous methanol in 100 mM TEAB, pH7.1; TEAB acidified to 7.1 using 85% phosphoric acid) was added in volumes 7 times that of the volume of protein extract being digested. Samples in which the addition of S-trap buffer would result in a total volume greater than 2 mL, were transferred to a 5 mL centrifuge tube (Protein LoBind, Eppendorf) with a rinse of the 2 mL tube with S-trap buffer to minimize sample loss. After addition of the S-trap buffer, the sample was loaded onto the S-traps in 600 µL aliquots. A vacuum extraction manifold (Waters) was used for this step and the subsequent washes of the S-trap. The S-traps were then washed with ten 500 µL volumes of S-trap buffer, and a final wash of 500 µL of 80% methanol. The first wash aliquot was used to rinse the sample tube to reduce sample loss. S-trap columns were removed, spun at 2000 x g, and moved to a clean 2 mL centrifuge tube. Protein captured on the S-trap columns was digested with trypsin (Thermo Scientific™ Pierce™ Trypsin Protease, MS Grade) (1:8-1:25 ratio trypsin to total protein) for 12-16 hours at 37 °C. The trypsin was loaded onto columns in a volume of 125 µl 50 mM TEAB at pH 8. Digested samples were then eluted off the S-trap column through a series of washes: 80 µL of 50 mM Ambic, 80 µL 0.2% aqueous formic acid, and 80 µL 50% acetonitrile containing 0.2% formic acid. Columns were spun down at 4000 g for 1 minute after each addition. The S-trap column was removed and peptide solutions were transferred to a 1.7 mL centrifuge tube (protein lobind, Costar) and dried down in a vacufuge (Eppendorf) for 2-4 hours (V-AQ setting). The dry peptides were then stored at -80°C until reconstitution. Dried peptides were reconstituted in a volume of 1% FA, 3% ACN to a concentration of

0.5 µg µL-1. Protein digestion was conducted by Lena Beckley, with assistance from Elden Rowland.

2.13 Liquid chromatography tandem mass spectrometry

Peptide extracts were desalted using 50 mg HyperSep C18 SPE Cartridges (Thermo Scientific). Cartridges were primed with 0.5 mL of methanol then 0.5 mL of 50% acetonitrile followed by equilibration with 1 mL 0.1% TFA. Samples were diluted with 0.1% TFA to a volume of ~0.2 mL and, loaded onto cartridges by positive pressure from a syringe then the flow through loaded a second time. The cartridges were washed 3 times with 1 mL of 0.1% TFA using a vacuum manifold. Peptides were eluted with 2 x 0.2 mL 50% acetonitrile, 0.1% FA, then 0.1 mL 70% acetonitrile, 0.1% FA with positive pressure from a syringe. The eluant was brought to dryness in a speed vac as described above.

Desalted samples were solubilized in 1% formic acid, 3% acetonitrile and analyzed by reverse phase liquid chromatography tandem MS (LC-MS/MS). 3 µl direct injections containing 1 µg of peptide digest were performed onto a 100 µm × 40 cm column containing 4 µm, 90 Å, Proteo C18 beads (Phenomenex, Torrance, CA), self-packed in a fused silica emitter tip (New Objective, Woburn, MA). Chromatography was performed using a Dionex Ultimate 3000 UHPLC (Thermo Scientific, San Jose, CA) at a flow rate of 0.25 µL/min. Peptides were separated using a gradient of 3–35% B over 75 min, then 30-55% B over 12 min, followed by 4 min at 95% B, where B solvent was 0.1 % formic acid in acetonitrile and A solvent was 0.1 % formic acid in HPLC grade water. Column outflow was interfaced to a Orbitrap LUMOS Tribrid with a Nanospray Flex ion source and FAIMS Pro ion mobility filter (Thermo Scientific, San Jose, CA). The ion spray voltage was 1800 V and ion transfer tube 300°C. FAIMS was operated with standard resolution and total carrier gas flow of 4.6 L/min. Three FAIMS compensation voltages were applied over a fixed 3 second cycle time, 1.2 sec at -50 V, 1.2 sec at -65 V and 0.6 sec at -80V.

Survey/precursor scans (MS1) were performed using the Orbitrap with a 400–1600 m/z mass range and 120,000 resolution (Profile mode, AGC target 100% - 4 e5, Max IT 50 ms - Auto, RF lens 30 %). Data dependent MS/MS scans were acquired in parallel in the iontrap (Centroid mode, ACG target 100% - 1 e4, Max IT 35 ms -

Dynamic, Rapid scan rate) with a 1.6 Da quadrupole isolation window and HCD fragmentation with 30% collision energy. Internal mass calibration with fluoranthene was performed at the beginning of each run using the RunStartEasyIC feature. Mass spectrometry was conducted by Elden Rowland.

Charge states from only 2 to 6 were fragmented and previously selected precursors were added to an exclusion list for 60 s (+/- 10 ppm). The minimum intensity threshold for MS2 selection was 5000 and ions were selected from most to least intense.

2.14 Protein identification and quantitative analysis

The acquired mass spectra were matched with peptide sequences from a metatranscriptome-derived reference database (see below) using MSGF+ within OpenMS (Kim & Pevzner, 2014; Röst et al., 2016). The reference database was appended with a database of common contaminants from the common Repository of Adventitious Proteins (The Global Proteome Machine Organization), and then removed redundant sequences using Python script by P. Wilmarth (github.com/pwilmart/fasta_utilities). The search was conducted using an 8-ppm precursor mass tolerance, and set cysteine carbamidomethylation as a fixed modification, and methionine oxidation and N-terminal glutamate to pyroglutamate conversion as variable modifications. Lastly, peptide-spectral matches were filtered at a 1% false discovery rate using a target-decoy strategy, where 'target' represents all the sequences in the database and 'decoy' represents all the database sequences in reverse (Elias & Gygi, 2007). Feature intensity (which approximates peptide abundance, roughly) was calculated based on MS1 ion intensity using FeatureFinderIdentification (Weisser & Choudhary, 2017). Note that peptide to MS1 peak area relationships are subject to multiple biases that prevent us from directly comparing peak area of small numbers of peptides to each other, though the abundance of individual peptides can be compared across treatments. Database searching was conducted by Loay Jabre.

2.15 Protein taxonomic assignments

Each identified peptide was given a taxonomic annotation. In certain cases, peptides received more than one taxonomic assignment. To resolve these annotations, we identified unique assignments at the lowest resolution possible. If a peptide was identified as belonging to several groups at a given level, it was deemed 'ambiguous' at that level,

and broader taxonomic classification was searched until a unique assignment was reached. This could be as broad as assigning a peptide as belonging to eukaryotes. Indeed, a large proportion of peptides could not be resolved further than eukaryotes and many of these had functional annotations which we may expect to be broadly shared across taxa, for instance from actin-related proteins, histones, and molecular chaperones.

As the focus of this work was examining the photosynthetic community (predominantly at the class level), any peptides belonging to non-photosynthetic eukaryotes, or belonging to photosynthetic eukaryotes which could not be resolved at the class level were assigned as 'other eukaryote'. Any bacterial peptides which were not assigned to Cyanophyceae at the class level were designated 'other bacteria'.

2.16 Protein fraction and expression calculations

Protein mass fractions were calculated by summing peptide abundances of a given functional allocation withing a group, divided by the total peptide abundance of that group. A 'greedy' approach was used combining KEGG, cog and KOfam functional annotations, whereby if any of the following identified a peptide as belonging to a functional group of interest, it was designated to that functional group. Ribosomal proteins were found by searching for functional annotations including "Ribosom/ribosom". Photosynthetic proteins included photosystems I and II, light-harvesting complexes, flavodoxin, plastocyanin, chlorophyll a-b binding proteins and chloroplast-associated ATPase. Single iron-stress proteins (Flavodoxin and Plastocyanin) expression was examined in Bacillariophyta and prymnesiophytes. The peptide intensity identified for each protein were summed and then divided by the taxon-specific total peptide abundance. All protein expression data analysis was performed by Lena Beckley.

2.17 16S rRNA gene amplicon sequencing

DNA was extracted using the Qiagen Allprep DNA/RNA kit. Sequencing of 16S rRNA gene amplicons was conducted at the Integrated Microbiome Resource (IMR) using an Illumina MiSeq (paired-end mode) of 300 bp. We used the V4-V5 universal primer targeting the 16S rRNA gene (Parada et al., 2016). Amplicon Sequencing Variants (ASVs) were determined using QIIME (version 2019.7) with established protocols as in (Robicheau et al., 2022). ASVs were initially classified using SILVA version 13 (Yilmaz et al., 2014), and 16S chloroplast ASVs were reclassified using PhytoREF (Decelle et al.,

2015). DNA/RNA extractions and 16S rRNA gene amplicon data analyses were conducted by Lena Beckley with the assistance of Rebecca Stevens-Green and Jennifer Tolman.

2.18 Comparison of 16S rRNA amplicon sequencing data

To compare the photosynthetic community composition between the metatranscriptome 2019 sites and the MetalGate 2021 experimental dataset, these samples were concurrently run through the QIIME pipeline, this allowed direct ASV-ASV comparisons between the two datasets. Reads were summed across all samples for both respective datasets and then ranked by most abundant ASVs. We used the top 50 most abundant ASVs in the 2019 dataset as a baseline cut-off to represent taxa very likely to be adequately represented in the metatranscriptome.

2.19 Metatranscriptome sample collection

Water collection for the 2019 metatranscriptome samples occurred July-August 2019 on the RV Maria S. Merian. Surface seawater (approximately at 2-3m depth) was collected from a towed sampling device equipped with acid-washed tubing and suction provided by a Teflon bellows pump. Samples were collected into acid-washed 10- or 20-L high density polyethylene (HDPE) carboys and filtered in a cold room (5 °C) sequentially onto 3.0 and 0.2 µm pore-size Isopore polycarbonate (PC) filters (47mm, Millipore) using a peristaltic pump and acid-washed Tygon and Silicon tubing. For each sample, approximately 1 L of seawater was filtered and filtration was completed within 45 mins of sample collection. Filters were stored in 2 mL cryovials, immediately shock-frozen in liquid nitrogen and stored at -80 °C. Sample collection was conducted by Insa Rapp.

2.20 RNA extraction (metatranscriptome)

RNA was extracted using the AllPrep RNA/DNA Mini Kit (Qiagen), following the manufacturer's protocol, with the exception of adding lysozyme and proteinase K prior to extraction. Individual size fractions of 0.2µm and 3 µm were eluted in 50µl. After combining same volumes of those fractions, samples were concentrated to a final volume of 30 µl using RNeasy MinElute Cleanup kit (Qiagen). RNA extraction was conducted by Martha Guzman.

2.21 RNA Library preparation and sequencing

Total RNA was quantified and its integrity was assessed on a LabChip GXII (PerkinElmer) instrument. rRNA was depleted from 250 ng of total RNA using QIAseq FastSelect (-5S/16S/23S Kit 96rxns and -rRNA Plant Kit). cDNA synthesis was achieved with the NEBNext RNA First Strand Synthesis and NEBNext Ultra Directional RNA Second Strand Synthesis Modules (New England BioLabs). The remaining steps of library preparation were done using and the NEBNext Ultra II DNA Library Prep Kit for Illumina (New England BioLabs). Adapters and PCR primers were purchased from New England BioLabs. Libraries were quantified using Kapa Illumina GA with Revised Primers-SYBR Fast Universal kit (Kapa Biosystems). Average size fragment was determined using a LabChip GXII (PerkinElmer) instrument. The libraries were normalized and pooled and then denatured in 0.05N NaOH and neutralized using HT1 buffer. The pool was loaded at 225pM on a Illumina NovaSeq S4 lane using Xp protocol as per the manufacturer's recommendations. The run was performed for 2x100 cycles (paired-end mode). A phiX library was used as a control and mixed with libraries at 1% level. Base calling was performed with RTA v3.4.4 . Program bcl2fastq2 v2.20 was then used to demultiplex samples and generate fastq reads. Library Preparation and sequencing was done at Genome Quebec.

2.22 Metatranscriptome database construction and annotation

The quality-checked metatranscriptome reads from the 3 samples were assembled using Trinity (Grabherr et al., 2011). Following assembly, the contigs were processed using a workflow based on the Anvi'O program (Eren et al., 2021). Briefly, the program prodigal (Hyatt et al., 2010) was used to identify Open Reading Frames (ORFs) or genes from the contigs. The genes were compared to databases such as KEGG (Kanehisa & Goto, 2000), COG (Tatusov et al., 1997), PFAM (Mistry et al., 2021) and KOFam (Aramaki et al., 2020) for functional annotations. Taxonomic assignments for the genes were obtained using EUKulele (Krinos et al., 2021) using MMETSP (Keeling et al., 2014) and MarRef (Klemetsen et al., 2018) databases. The gene sequences, translated peptides and all relevant information related to the gene sequences was exported as tables from Anvi'O and converted into a custom database flatfile using the python scripts from the DoT_Gene_Database repository

(https://github.com/MichaelWright44/DoT_Gene_Database). Database generation was conducted by Dhwani Desai and Martha Guzman.

2.23 Statistical Analysis and Plotting

Statistical analyses and plots were generated using R version 4.2.3. and R Studio 2023.03.0. Statistical analysis of bioassay responses was conducted using two-way ANOVAs with interaction terms for iron and temperature responses. Maps were generated using ggOceanMaps (Vihtakari, 2022).

Chapter 3: Results

3.1 Study site: Irminger Basin

The MetalGate cruise circumnavigated Iceland and sampled its surrounding seas July-August 2021 (Figure 1). This thesis focuses on the Irminger Basin (stations 2, 4, 6, and 7, Figure 1), with a particular focus on the bioassay experiment conducted at station 4. Station 2 was opportunistically revisited roughly a month after its initial sampling and is referred to here as 'Station 2 Reoccupied'. For peptide identification via the metaproteomics pipeline, we used a metatranscriptome collected from this region in July 2019; sites which contributed to the metatranscriptome are shown in yellow (Figure 1).

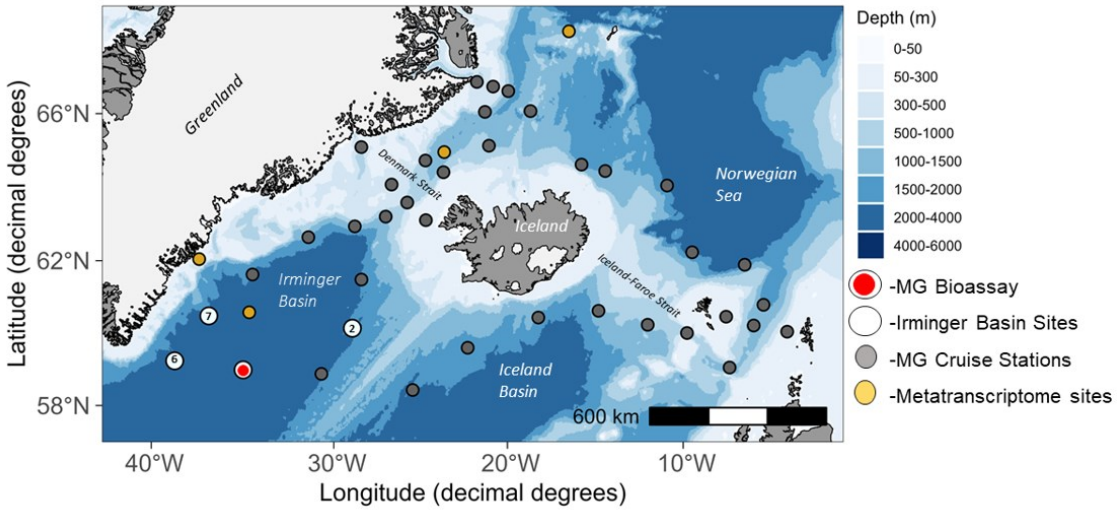

Figure 1. Map indicating MetalGate cruise track and sites of the 2019 metatranscriptome collection. White sites indicate Irminger Basin stations that are included in this thesis. Grey sites indicate MetalGate (MG) cruise stations not included in this thesis (the complete MG cruise track). Yellow sites indicate where sample collection occurred for the 2019 metatranscriptome.

3.2 Irminger Basin baseline conditions

Baseline conditions encountered in the Irminger Basin were broadly uniform between stations (Figure 2). Moderate levels of leftover surface nitrate were consistently observed at stations 2, 6 and 7 (6-7 µM NO_3^-). Surface silicate concentrations ranged from 1.5-2 µM. Surface phosphate concentrations were consistently ~0.5 µM. Low concentrations of dFe at surface were encountered at all Irminger Basin stations (~0.05-0.16 nM Fe). Moderately low surface concentrations of dMn were also observed at all Irminger Basin stations (0.44-0.47 nM Mn). Relative Fluorescence Units (RFU) values

peaked near 20-30m for stations 2, 6 and 7. Pigments were dominated by C3 flagellates (a grouping including haptophytes and pelagophytes). Station 2 was reoccupied approximately a month after its first sampling. Macronutrient concentrations were somewhat drawn down from initial sampling, however a pool of surface nitrate remained (4.3 µM NO_3^-). Moderate concentrations of surface silicate (~1.7 µM) and phosphate (0.34 µM) also were observed at station 2 reoccupied.

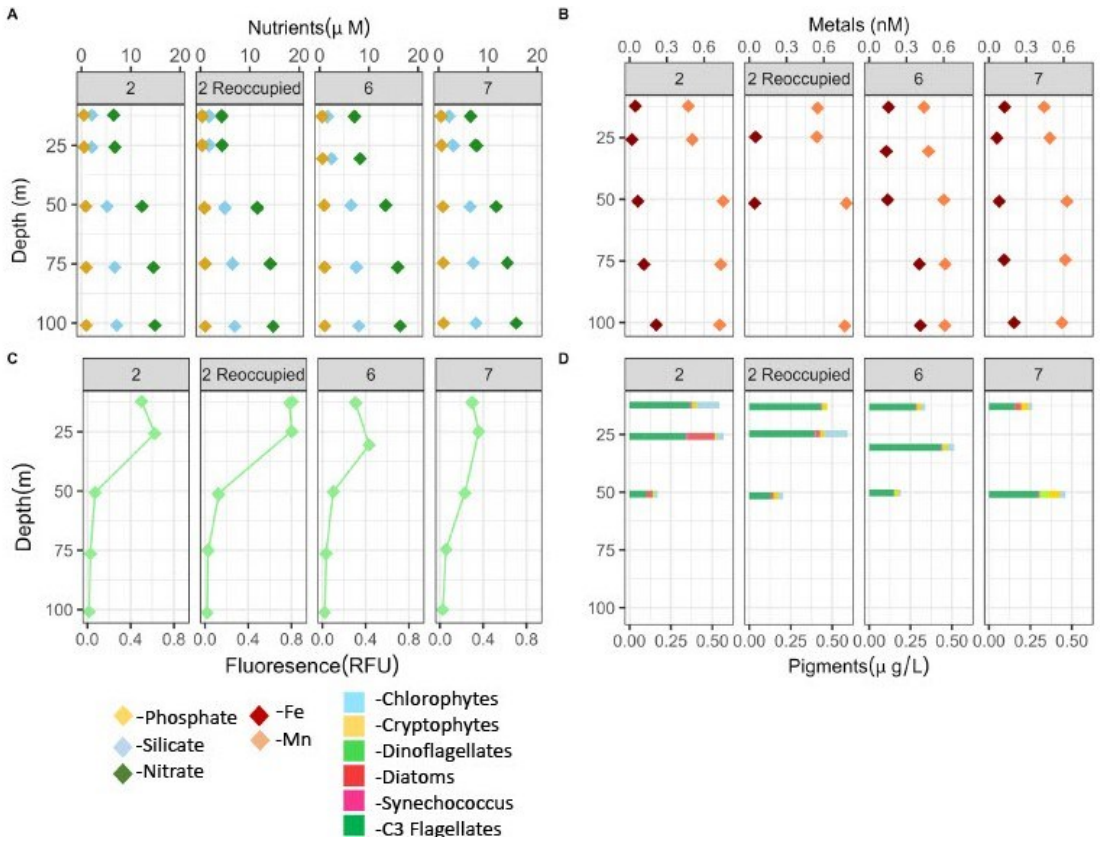

Figure 2. Depth profiles of nutrients, trace metals, fluorescence, and pigments in the Irminger Basin, 2021. A-Macronutrient profiles in the first 100m (nitrate, phosphate and silicate) at stations 2, 2 Reoccupied, 6 and 7 B- Dissolved trace metal concentrations in the first 100m (Fe and Mn) at stations 2, 2 Reoccupied, 6, and 7 C-Depth profile of chlorophyll in relative fluorescence units (RFUs) in the first 100m D-Depth profile of CHEMTAX derived pigment groups in the first 50m. Station 2 Reoccupied is station 2 revisited ~1 month later.

3.3 Database suitability

Metaproteomic analyses hinge on utilizing representative databases to identify detected peptides and match them to organisms and functions (McCain et al. 2022). Previous work (Jabre et al., in prep) has shown promising results for using unpaired meta transcriptome-derived databases in Southern Ocean metaproteomics, finding that the use of a database for matching peptides in one part of the Southern Ocean can be done using a deeply sequenced metatranscriptome from another Southern Ocean region. Here we interrogated the suitability of using an unpaired metatranscriptome for these analyses in the North Atlantic, in this case from the same region and season, but two years prior, and from surface samples only (Figure 1). First, we used 16S rRNA gene amplicon sequencing to compare the dominant photosynthetic community members from the 2019 sampling to our 2021 sampling. Second, we evaluated the proportion of mass spectra collected in our 2021 efforts that were identified using the 2019 database, as described below.

The first approach we used to assess the 2019 metatranscriptome database suitability was a comparison of the photosynthetic community composition between the 2019 and 2021 sampling. We did this by comparing chloroplast and cyanobacterial 16S rRNA gene amplicon sequence variants (ASVs) between the 2019 and 2021 datasets. For the 2021 dataset we examined samples at T_0 and T_f of the bioassay experiment. For the 2019 dataset, all samples from all sites which contributed to the 2019 metatranscriptome creation were included in this analysis. Our goal was to determine how well-represented we expect the overall 2021 photosynthetic community to be in the 2019 metatranscriptome. To determine this, we ranked the most abundant ASVs for each dataset and then examined how many ASVs from 2021 were paired with the 50 most abundant ASVs from the 2019 dataset, and determined their contribution to total read counts (Figure 3). Overall, we found that of the top 50 most abundant ASVs in the 2019 metatranscriptome samples, 40 of these ASVs were also found in the 2021 dataset and represented 73% of all reads in the 2021 dataset. Of the top 10 most abundant 2021 ASVs, 8 were also found in the 2019 top 50 most abundant ASVs. This subset of top 10 2021 ASVs represented 59% of all 2021 reads (Figure 3). Thus, we were reasonably confident that the 2019 database had adequate coverage of the most abundant

photosynthetic community members within the 2021 dataset, and we proceeded to use the 2019 database for database searching peptide IDs.

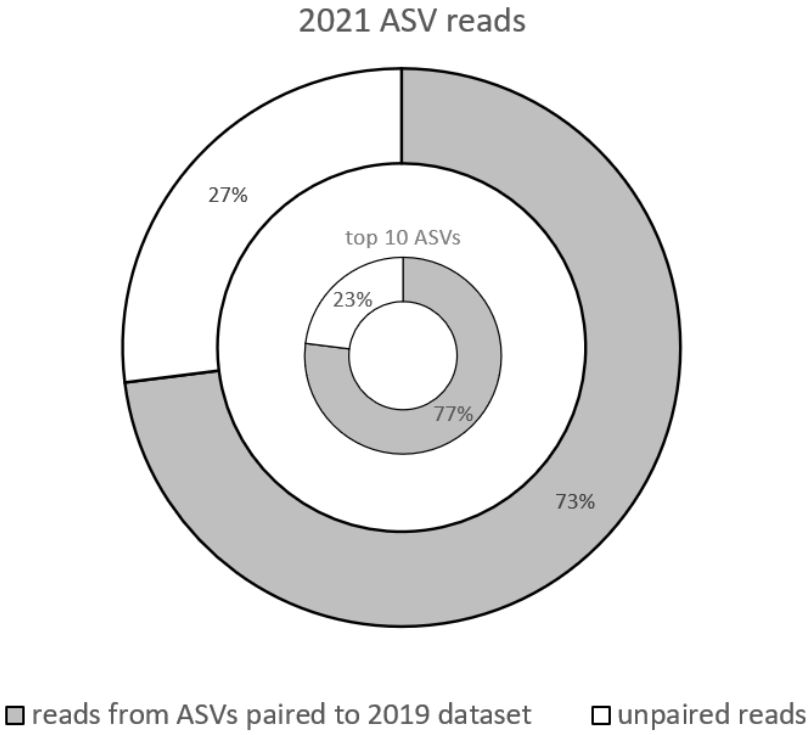

Figure 3. The percentage of reads from chloroplast and cyanobacterial 16S amplicon sequence variants (ASVs) which matched between the 2021 dataset and the 50 most abundant ASVs in the 2019 dataset. Outer circle-the percentage of total 2021 reads from ASVs paired in the 2019 dataset. Inner circle-the percentage of the 10 most abundant ASVs in the 2021 dataset that paired to top 50 ASVs in the 2019 dataset.

Database searching is a critical step in metaproteomics to match observed mass spectra to theoretical spectra generated from possible protein sequences, predicted using a metatranscriptome, to ultimately determine peptide sequences, origin, and function. Our database searching resulted in 48,294 unique peptide IDs across all experiment and depth profile samples. We evaluated the quality of the database matching by examining the proportion of the mass spectrometry signal that could be matched with a peptide sequence. Assessment of the proportion of Total Ion Current (TIC, which represents the material observed via mass spectrometry, which we expect to be mostly protein) that was matched to a peptide ID in this study, revealed a marked depth-dependence in field

samples (Figure 4). Samples above 50m had relatively high percentages of TIC accounted for by matched peptides, which were variable, between 17-55%, and averaged 21%. Samples taken at 50m and below showed a sharp decline in TIC matched, ranging from 4-12% and averaging 9%. Work in the Arctic and Atlantic using paired metatranscriptomes (i.e a metatranscriptome assembled from samples taken from the same water mass), have found that ~25-30% (Rapp et al., in prep) and ~40% (White et al., in prep) of TIC was matched to a peptide ID. Based on these paired database metrics we determined our match rates within the first 40m were sufficient for downstream analyses. The metatranscriptome database was deemed unsuitable for reasonable quantitative evaluation of deeper samples, and subsequent metaproteomic analyses were conducted for the first 40m only.

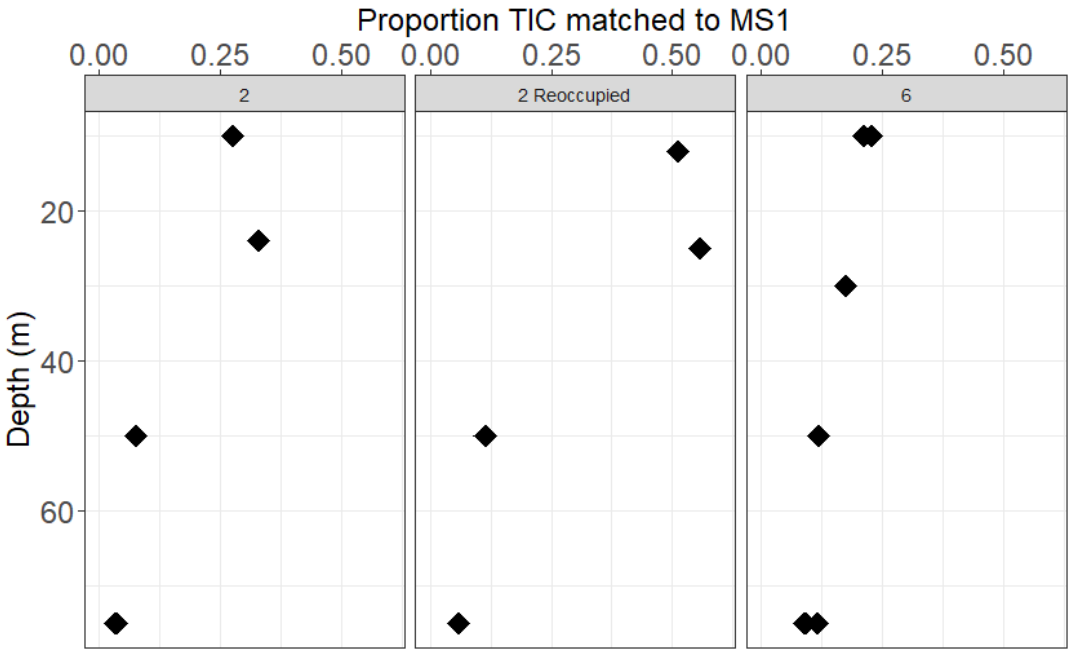

Figure 4. The proportion of total ion current (TIC) that was matched to a peptide ID after database searching, through the water column (0-75m) at stations 2, 2 Reoccupied, and 6. TIC represents the total material observed via mass spectrometry (which we expect to be mostly protein), MS1 represents the total material observed via mass spectrometry, which was matched to a peptide ID. The proportion of TIC matched to MS1 is the proportion of total material observed via mass spectrometry which was matched to a peptide ID.

3.4 Irminger Basin protein-based community composition

The microbial community composition in the Irminger Basin as revealed through metaproteomics showed a rather consistent surface community across stations. To examine community composition with metaproteomics, peptide abundances were pooled at the class level, normalized by the total identified peptide abundance per sample. If a peptide could not be resolved to class, it was resolved by the next most precise taxonomy, and then assigned to a broader pool such as 'other eukaryote', or 'other bacteria'. Major contributions to the photosynthetic community included Bacillariophyta, Prymnesiophyceae and Dinophyceae, each contributed on average just under 4% of the total identified peptide abundance in field samples (Figure 5). Smaller contributions included Cryptophyceae, Cyanophyceae and Pelagophyceae, all contributing on average less than 2% of the total identified peptide abundance across field sites (Figure 5). Much of the protein identified at field sites were from eukaryotes which were either not able to be further resolved (i.e ambiguous eukaryotes), or from heterotrophic eukaryotes, which were not the focus of our inquiry here, for instance Spirotrichea ciliates. Oftentimes peptides which were identified as ambiguous at the eukaryotic level came from proteins which we may expect to be broadly shared across taxa, for instance from actin-related proteins, histones, and molecular chaperones. Ambiguous and other eukaryotic peptides combined contributed between 50-78% of the total community composition across field sites (Figure 5).

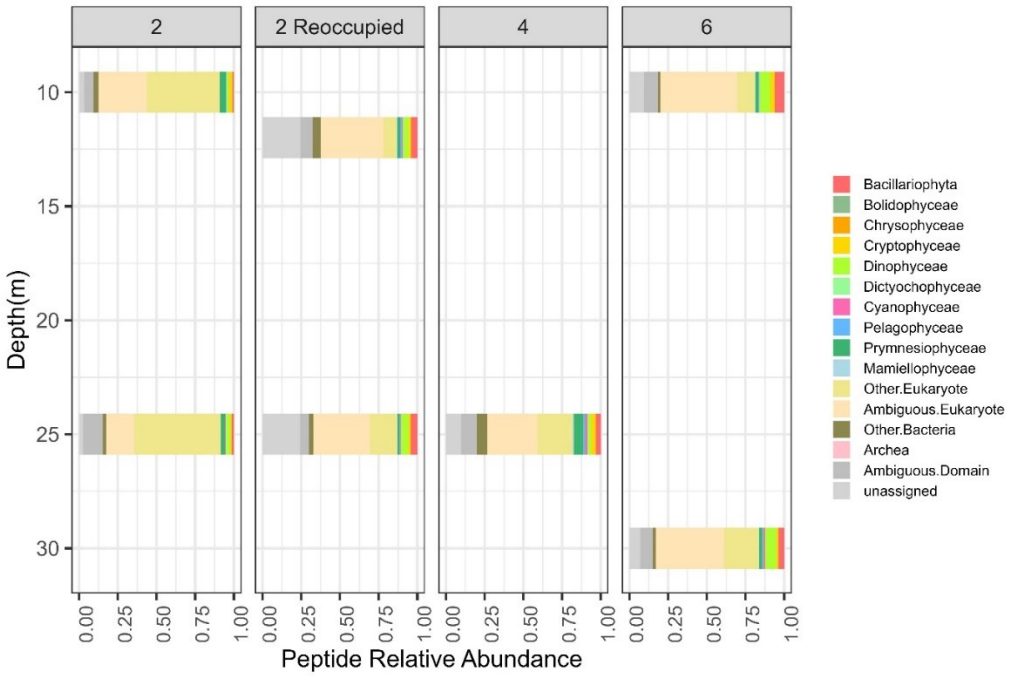

Figure 5. Relative contributions of different taxa to identified peptide abundance at field sites 2, 2 Reoccupied, 4 and 6 based on untargeted metaproteomics. Relative abundance is calculated by normalizing peptides by the total identified peptide abundance per sample and grouping by taxa.

Two of the most abundant phytoplankton groups found in the Irminger Basin were Bacillariophyta and Prymnesiophyceae. We further examined the composition of each, at the genus level across depth-profiles in the Basin. *Pseudo-nitzschia* contributed on average 34% of total bacillariophyte protein across initial sampling of the Basin, however dropped to 6% upon reoccupation of station 2 (Figure 6). *Thalassiosira* contributed on average 5% to total bacillariophyte protein upon initial sampling of the Basin but increased to 35% at reoccupation of station 2. Prymnesiophyceae composition remained rather consistent across the Basin and sampling periods, with the notable exception of increased abundance of *Coccolithus* at station 6. Generally, prymnesiophyte protein was dominated by *Phaeocystis* (45% on average), and *Chrysochromulina* (26% on average) (Figure 6).

Figure 6. Group-normalized protein contributions of Bacillariophyta and Prymnesiophyceae protein across field stations 2, 2 reoccupied, 4 and 6 from 0-30m. Peptide abundances were normalized by the sum of peptide abundances from each respective group (Bacillariophyta and Prymnesiophyceae) and pooled at the genus level.

Any genus which contributed less than 1% across all samples are included in each figure but shown in beige. A-Bacillariophyta peptides B-Prymnesiophyceae peptides.

3.5 Biogeochemical bioassay results

A bioassay, manipulating temperature and iron availability, was conducted at station 4. Water for the bioassay experiment was collected at 25m depth. Nutrient drawdown and bulk physiological changes were observed in treatments throughout the five-day duration of the bioassay experiment, in which iron availability and temperature were manipulated (Figure 7). Nitrate, Phosphate and Silicate drawdown all had a pronounced iron effect ($p<0.001$) (S2). Nitrate concentrations were drawn down from 7.7 μM$\pm$0.03 at T_0 to 2.7 μM $\pm$1 in the *in situ* temperature +Fe treatment, and 0.06 μM$\pm$0.01 in the +4°C +Fe treatment. A much more pronounced nitrate pool remained at T_f in both the +4°C (5.5 μM $\pm$0.2) and *in situ* temperature (6.4 μM$\pm$0.5) treatments. Temperature also had a main effect on nitrate drawdown ($p<0.001$), the interactive effect of temperature and iron on nitrate drawdown was significant at ($p<0.05$). Iron had a main effect on silicate drawdown with starting concentrations of 2 μM $\pm$0.03, and final concentrations of 0.1 μM$\pm$0.06 in +4°C +Fe and 0.69 μM$\pm$0.2 in *in situ* temperature +Fe treatments, while controls at both temperatures had markedly less silicate drawdown, to final concentrations of 1.6 μM$\pm$0.09 at *in situ* temperature, and 1.3 μM $\pm$0.04 in the +4°C treatment. F_v/F_m values represent the maximum quantum yield of PSII and are widely used as a diagnostic for photosynthetic efficiency and nutrient stress in phytoplankton. F_v/F_m values at T_0 were 0.32 $\pm$0.01, they increased in +Fe treatments at T_f to be 0.47 $\pm$0.04 for the *in situ* temperature +Fe treatment, and 0.46$\pm$0.004 for the +4°C +Fe treatment. Temperature did not have a significant effect on T_f F_v/F_m but iron did at ($p<0.001$). Starting Chl-a values were 0.51 μg/L $\pm$0.06 and increased in the +Fe treatments to 2.6 μg/L $\pm$0.4 for *in situ* temperature +Fe and 4.7 μg/L $\pm$0.8 in the +4°C+Fe treatment. Both temperature treatments without added Fe did not see the same magnitude of increased Chl-a. The *in situ* temperature treatment at T_f decreased slightly to 0.46 μg/L $\pm$0.2, and the +4°C had a slight increase to 0.71 μg/L $\pm$0.02. Iron had a significant main effect on T_f Chl-a ($p<0.001$). Fe treatments were amended with ^{57}Fe, leftover amounts of ^{57}Fe (0.29-0.44 nM) can be seen in the +Fe treatments and not the controls.

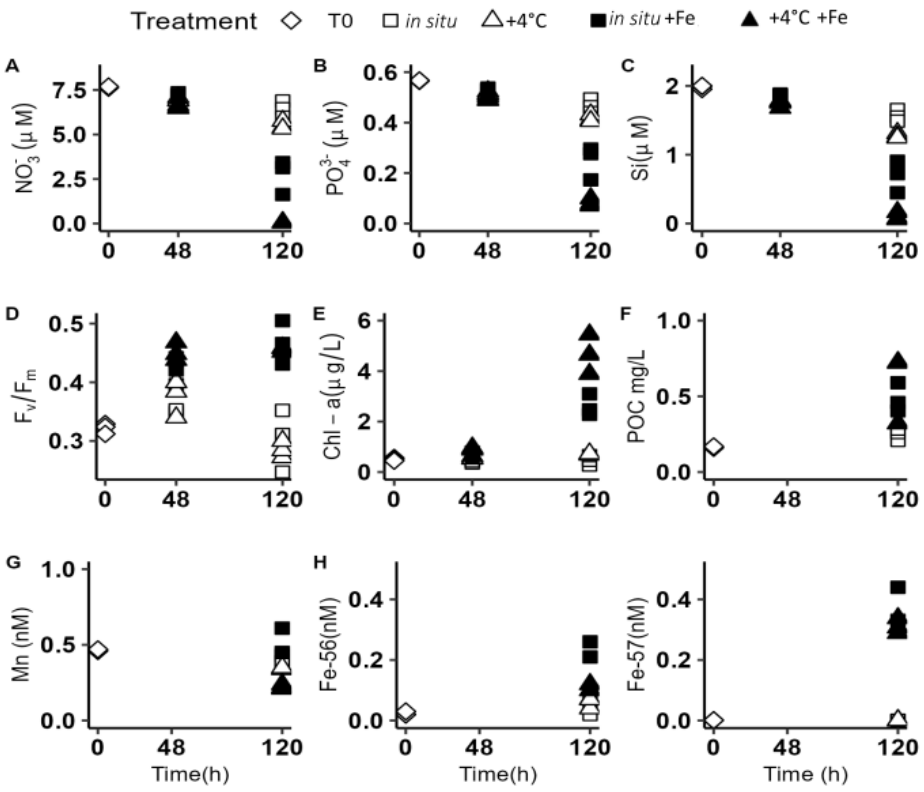

Figure 7. Biogeochemical responses to a five-day Fe-temperature bioassay experiment. A- Nitrate values at T_0, T_{48} and T_f of the bioassay measured onboard using a flow QuAAtro Auto-Analyzer, B- Phosphate values at T0, T_{48} and T_f of the bioassay measured onboard using a flow QuAAtro Auto-Analyzer, C-Silicate concentrations measured at T_0, T_{48} and T_f of the bioassay, D- F_v/F_m values at T_0, T_{48} and T_f of the bioassay measured onboard using FRRf , E- Chl-a concentrations at T_0, T_{48} and T_f of the bioassay, F- POC values at T_0 and T_f of the bioassay, G- Dissolved Mn measurements at T_0,and T_f H- Dissolved ^{56}Fe measurements at T_0,and T_f, F, Dissolved ^{57}Fe measurements at T_0,and T_f.

3.6 Bioassay results-Community Composition

We examined changes to the community composition throughout the experiment with three approaches. We assessed shifts in the relative abundance of the photosynthetic microbial community classes by examining chloroplast and cyanobacterial 16S rRNA gene ASVs. We also used CHEMTAX-derived pigment data to assess shifts in the photosynthetic community. Through untargeted metaproteomics, we examined the entire microbial community composition.

One of our assessments of community composition shifts in the bioassay experiment leveraged chloroplast and cyanobacterial 16S rRNA gene ASVs to examine changes to the phytoplankton community (Figure 8). We examined ASVs at the class designation, all ASV reads were normalized to the total reads per sample, and then grouped by class. The percent of reads mapped to ASVs assigned to Bacillariophyta increased from 23%±5 at T_0, to 44%±4 at T_f in the *in situ* temperature +Fe and 47%±3 in the +4°C +Fe treatments. This increase in proportion of Bacillariophyta reads was not observed in the controls at T_f, with 26%±7 (*in situ* temperature) and 25%±7 (+4°C). The percent of ASV reads assigned to pelagophytes was 11%±1 at T_0, remained nearly constant in the *in situ* temperature 11%±2 and increased slightly in the *in situ* temperature +Fe treatment 14%±7 at T_f. Decreases were observed in both the high temperature treatments to 6%±1 in the +4°C and 9%±2 in the +4°C +Fe at T_f. Reads assigned to Cyanophyceae were 45%±10 at T_0 and decreased in all treatments at T_f. The largest decrease in Cyanophyceae contribution was observed in the *in situ* temperature +Fe treatment to 13%±5 at T_f. The relative Cyanophyceae contribution was similar in the *in situ* temperature (18%±2) and +4°C +Fe (18%±1) treatments. The treatment which saw the least decline in relative Cyanophyceae contribution was +4°C with 36%±5 at T_f. Reads assigned to Prymnesiophyceae contributed 17%±5 at T_0, and increased in all treatments. The largest increase in Prymnesiophyceae contribution was in the *in situ* temperature treatment (33%±4), then the +4°C treatment (26%±3). Slight increases were seen in both iron treatments with 21%±4 in the *in situ* temperature +Fe and 19%±2 in the +4°C +Fe treatment at T_f (Figure 8). The majority of prymnesiophyte ASVs were not resolved further than class level (85% averaged across samples).

We also assessed shifts in the photosynthetic community as revealed through pigments. Diatoms made up a small percentage of overall pigment contributions at T_0 (3%±6) and increased in all treatments (33%±2 *in situ* temperature, 26%±6 +4°C), but was most pronounced in the iron treatments with 67%±5 in the *in situ* temperature +Fe and 68%±6 relative diatom pigment contribution in the +4°C +Fe treatments at T_f (Figure 8). Synechococcus pigments made up a rather small percentage of pigments never contributing more than 2% across all T_0 and T_f samples. C3 Flagellates made up the

majority of pigments at the beginning of the experiment 85%±5, and decreased in all treatments, to 57%±5 in the *in situ* temperature treatment and 64%±6 in the +4°C treatment at T_f. A more pronounced decrease was seen in the iron treatments with 25%±4 in the *in situ* temperature +Fe and 26%±5 C3 flagellate relative pigment contribution in the +4°C +Fe treatment at T_f (Figure 8).

Through metaproteomics we were able to assess the entire microbial community composition via peptide abundances, grouped at the class level and normalized by the total identified peptide abundance per sample. If a peptide could not be resolved to class, it was resolved by the next most precise taxonomy. The relative contribution of Bacillariophyta to total protein was 3%±0.5 at T_0 and increased to 26%±4 at T_f for the *in situ* temperature +Fe and 31%±3 at T_f for +4°C +Fe (Figure 8). Relative contribution of Bacillariophyta to total identified protein increased marginally in the controls to 9%±2 for *in situ* temperature and 7%±1 for the +4°C. Cyanophyta contribution to total identified protein did not exceed 2% for any of the treatments, or at T_0. Pelagophyte contribution to total identified protein also did not exceed 2% for any of the treatments. Prymnesiophyte contribution to total identified protein was 6%±2 at T_0 and increased in both the low temperature treatments 9%±3 *in situ* temperature and 7%±3 *in situ* temperature +Fe. Prymnesiophyte contribution to total identified protein remained the same or decreased slightly in the high temperature treatments to 6%±2 in the +4°C and 4%±1 in the +4°C +Fe treatment (Figure 8). Ambiguous eukaryote contribution to total identified protein was rather consistent across timepoints and treatments and made up on average 29%±5 across all experimental samples. Non-cyanobacterial bacteria made up on average 8%±3 of total identified protein across samples (Figure 8).

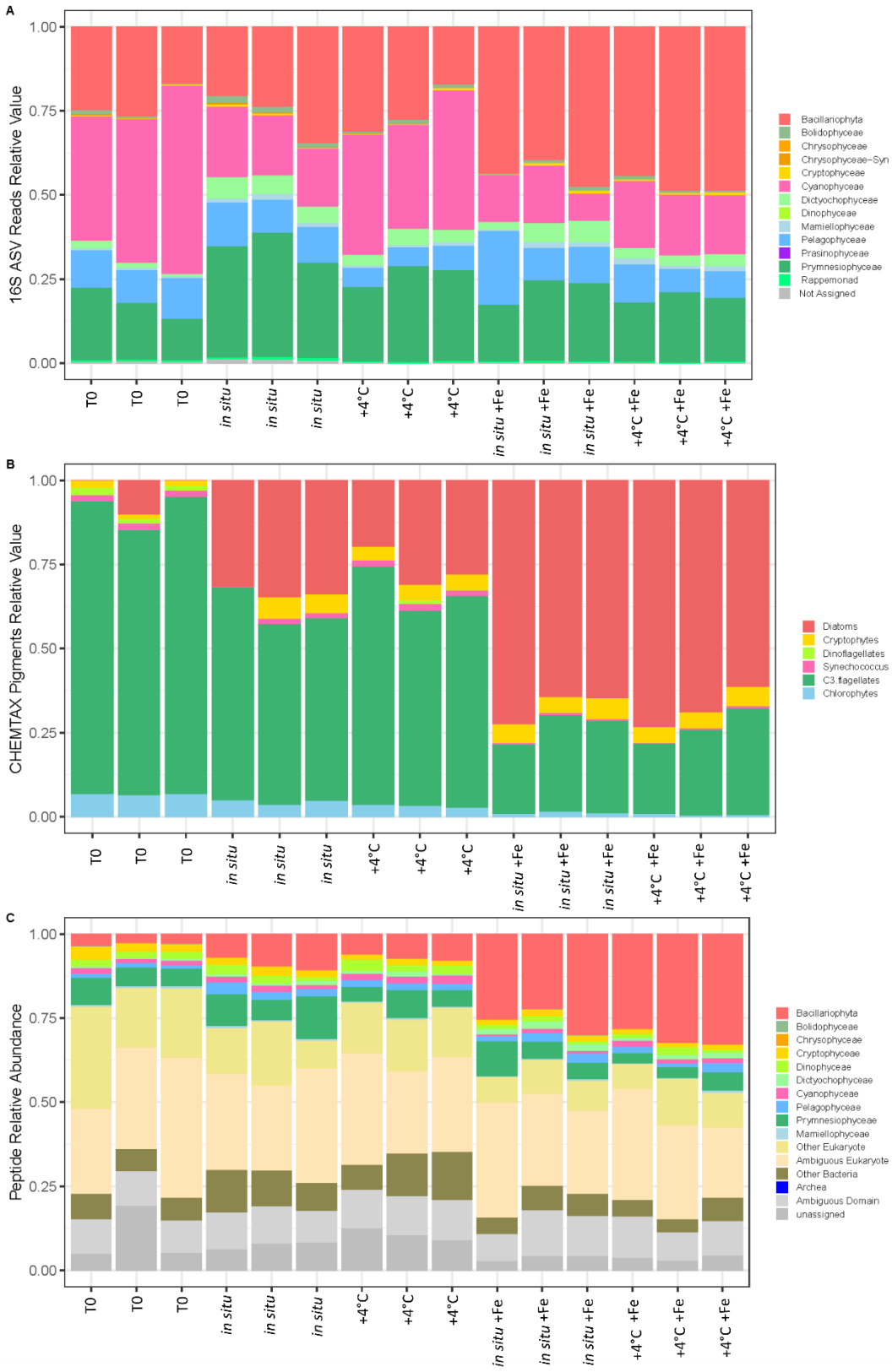

Figure 8. Microbial community composition at T_0 and T_f of the bioassay experiment with a focus on phytoplankton. A-relative abundance of chloroplast and cyanobacterial 16S

rRNA gene amplicon reads by class B-CHEMTAX derived relative contribution of pigments normalized to chl-a C-Relative peptide abundance per taxa, calculated by normalizing peptide abundances to the total peptide abundance per sample.

To assess the community of our two most abundant photosynthetic groups we used peptides to examine Bacillariophyta and Prymnesiophyceae proteins at the genus level across the bioassay samples. Taxonomic analysis at this grain across experimental samples had two goals: Firstly, to reveal any genus-level responses to the experimental bioassay conditions and secondly, to determine the taxonomic resolution that should be used to conduct additional metaproteomic analyses.

Although the contribution of Bacillariophyta protein to the whole community shifted throughout the duration of the experiment, the composition of this group remained rather consistent between timepoints and treatments. The dominant Bacillariophyta genus was *Pseudo-nitzschia*, ranging from 25-44% of the diatom community, with an average of 37%$\pm$4 across T_0 and T_f samples (Figure 9). *Chaetoceros, Fragilariopsis and Nitzschia* each constituted on average ~5% of the diatom community. The remaining bulk of the community (25% on average) could not be resolved any further than Bacillariophyta.

The dominant contributors to Prymnesiophyceae protein were *Phaeocystis* and *Chrysochromulina*, each made up on average 19% of the prymnesiophyte class across T_0 and T_f samples (Figure 9). However, there was a larger spread of relative contributions of these two groups within prymnesiophytes. The relative contribution of *Phaeocystis* ranged from 7-44% of prymnesiophyte peptides. *Chrysochromulina* ranged from 8-28% of prymnesiophyte peptides. The genus *Emiliania* contributed on average 3% to prymensiophyte protein. On average half of the peptides assigned to prymnesiophytes could not be resolved further than class level (50%$\pm$14) (Figure 9).

Both Bacillariophyta and Prymnesiophyceae had relatively high proportions of protein that could not be resolved further than class level. The composition of Bacillariophyta was extremely consistent across samples. Although the composition of Prymnesiophyceae was more varied across samples, there did not appear to be any dramatic community shifts in response to treatments. Based on this, and the fact that our next metaproteomics analysis steps are best conducted using large pools of proteins, we

determined that subsequent analyses should be conducted at the grain of these two broad groups (Bacillariophyta and Prymnesiophyceae).

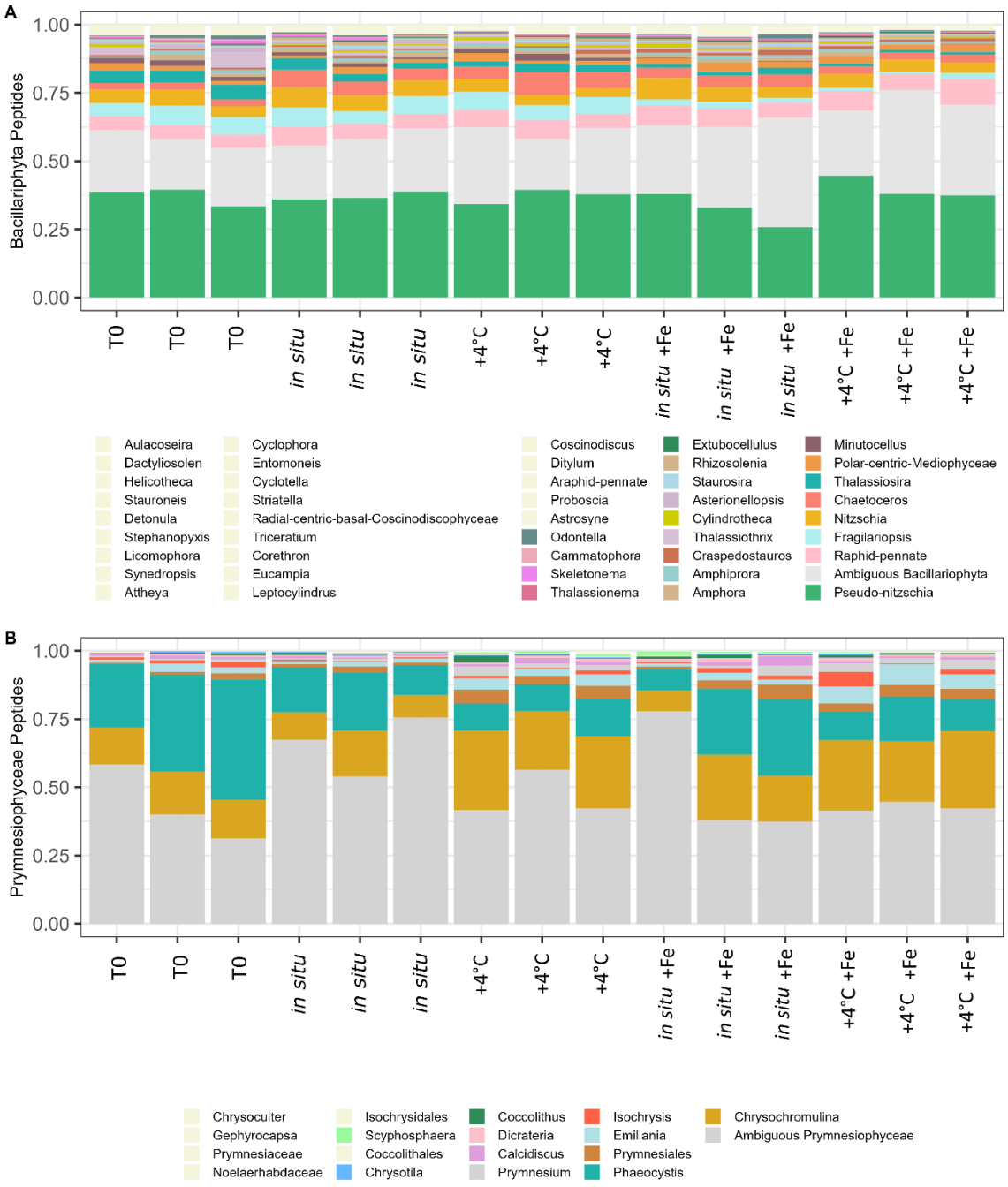

Figure 9. Group-normalized protein contributions to Bacillariophyta and Prymnesiophyceae at T_0 and T_f of the bioassay experiment. Peptide abundances were normalized to the sum of all identified peptide abundances from each respective group (Bacillariophyta and Prymnesiophyceae) and pooled at the genus level. Any genus which contributed less than 1% across all samples are included in each figure but shown in beige. A-Bacillariophyta peptides B-Prymnesiophyceae peptides.

3.7 Protein allocation to cellular functions

To examine proteomic allocation strategies of our two most abundant photosynthetic groups, we assessed the ribosomal and photosynthetic protein fractions, or the proportion of total protein allocated to these two key functions, in Bacillariophyta and Prymnesiophyceae. For the purposes of this analysis, photosynthetic protein fraction is inclusive of the light-dependant reactions only. A total of 4954 taxon-specific peptides were identified for Bacillariophyta. Of these Bacillariophyta peptides, 588 were identified as ribosomal and 270 were identified as relating to photosynthesis. We found 4419 taxon-specific peptides for Prymnesiophyceae. A total of 468 prymnesiophyte peptides were identified as ribosomal and 397 were identified as relating to photosynthesis (see S3 for list of n peptides in groups).

Bacillariophyta ribosomal protein fractions saw a main affect with iron ($p<0.001$), and temperature ($p<0.05$) (Figure 10, S4). Prymnesiophyceae ribosomal protein fractions did not have any statistically significant temperature or iron effects (S5). Both Bacillariophyta and Prymnesiophyceae ribosomal protein fractions saw the highest values in the *in situ* temperature +Fe treatment at T_f.

The Bacillariophyta photosynthetic protein fraction did not see any statistically significant effects from either iron or temperature (Figure 10). Prymnesiophyceae photosynthetic protein fractions did not see any statistically significant iron or temperature effects (S4). In prymnesiophytes the highest photosynthetic protein fractions were observed in the higher temperature treatment under both iron conditions.

Protein fractions for rubisco, the key Calivn cycle enzyme, were also calculated. A total of 46 rubisco peptides were identified in Bacillariophyta, 67 rubisco peptides were identified in Prymnesiophytes. Rubisco protein fractions had no significant effects from either iron treatment or temperature in Bacillariophyta (Figure 10). However, on average

the highest values for both iron conditions were found in the high temperature treatment. Rubisco protein fractions for prymnesiophytes did see a significant temperature effect ($p<0.05$), but no significant iron effects.

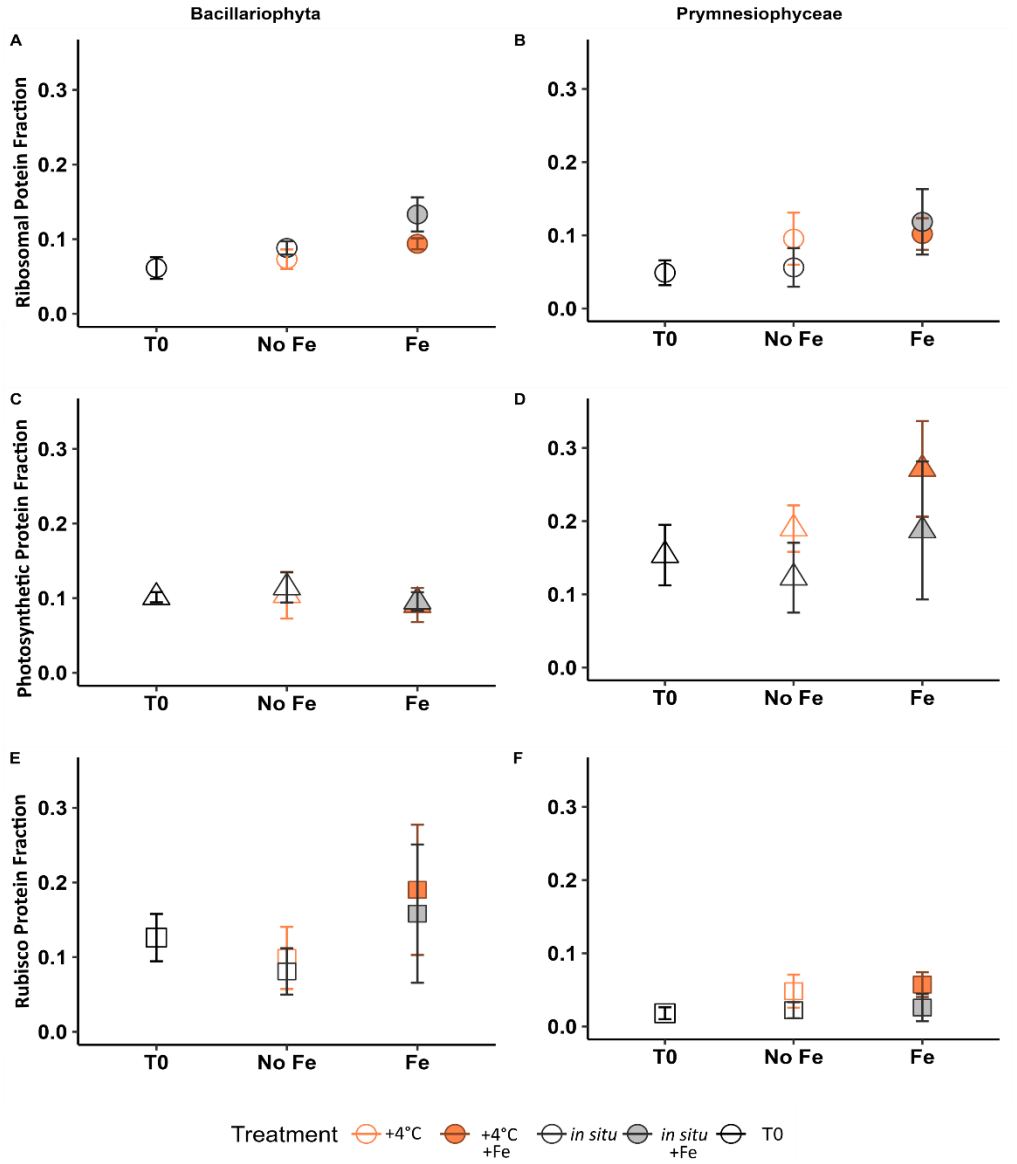

Figure 10. Group-normalized protein fractions for ribosomal proteins, photosynthetic proteins, and rubisco in Bacillariophyta and Prymnesiophyceae. A-Bacillariophyta ribosomal protein fraction B-Prymnesiophyceae ribosomal protein fraction C-Bacillariophyta photosynthetic protein fraction D-Prymnesiophyceae photosynthetic protein fraction E-Bacillariophyta rubisco protein fraction F-Prymnesiophyceae rubisco protein fraction. See S3 for overall n peptides identified for each taxa, S6 for sample-

specific n peptides identified in Bacillariophyta, S7 for sample-specific n peptides identified in Prymnesiophyceae.

Protein allocation to ribosomal proteins, photosynthetic proteins and rubisco were also assessed in Bacillariophyta and Prymnesiophyceae at all field stations. Bacillariophyta ribosomal protein fractions at field stations ranged from 4-22% (Figure 11). The highest values were observed at station 6, all other stations reported ribosomal protein fractions contributing less than 10% of Bacillariophyta protein. The photosynthetic protein faction in Bacillariophyta ranged from 7-13% across field sites. The Bacillariophyta rubisco protein fraction ranged from 3-14% across field samples. The lowest values for rubisco protein fractions were found at station 2. The ribosomal protein fraction in prymnesiophytes ranged from 5-15% in field samples. The photosynthetic protein fraction in prymnesiophytes ranged from 5-16% of prymnesiophyte protein in field samples but was 11% on average. The rubisco protein fraction in prymnesiophytes ranged from 2-5% across field samples (Figure 11).

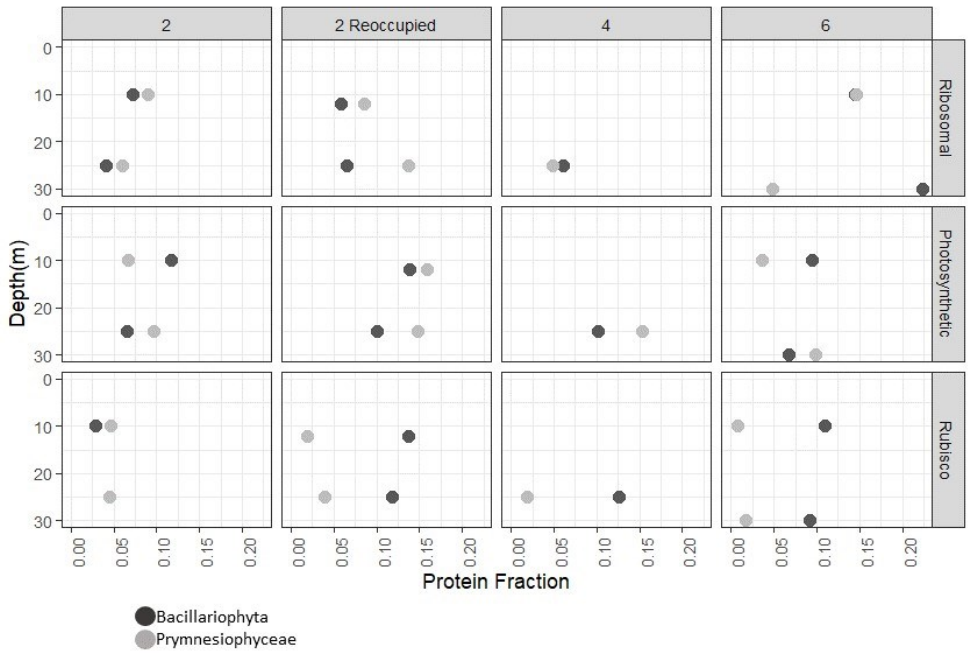

Figure 11. Group-normalized protein allocation to ribosomal proteins, photosynthetic proteins and rubisco in Bacillariophyta and Prymnesiophyceae at stations 2, 2 Reoccupied, 4 and 6 from 0-30m depth.

3.8 Photosynthetic protein allocation patterns

In addition to the bulk photosynthetic protein allocation analysis, we assessed proteomic allocation to different components of the light-dependent photosynthetic pool. Here, we examined how PSI, PSII, chloroplast-associated ATPase, flavodoxin and plastocyanin contributions to the photosynthetic protein pool changed in our two dominant photosynthetic groups (Bacillariophyta and Prymnesiophyceae) in the bioassay experiment.

In Bacillariophyta at T_0 plastocyanin contributed 36%±5 to the photosynthetic protein pool (Figure 12). Plastocyanin was nearly unchanged in the *in situ* temperature treatment (37%±6) and decreased slightly in the +4°C treatment (32% ±8). Both +Fe treatments saw declines in plastocyanin contribution to photosynthetic protein. Plastocyanin contribution decreased to 11%±2 in the *in situ* temperature +Fe treatment and 13%±5 of photosynthetic protein in the +4°C +Fe treatment. Flavodoxin protein contribution to the photosynthetic pool was 19%±2 at T_0 in Bacillariophyta. Flavodoxin contribution to the photosynthetic pool increased in both the controls to 34%±3 in the *in situ* temperature treatment and 34%±4 in the +4°C treatment. Flavodoxin contribution to the photosynthetic pool decreased in both the iron-amended treatments to 9%±1 in the *in situ* temperature +Fe and 8%±2 in the +4°C +Fe treatment. The protein contribution of PSI to the photosynthetic pool at T_0 was 0.5%±0.4 in Bacillariophyta. PSI contribution remained below 1% in both controls but increased to 7%±2 in the *in situ* temperature +Fe and 9%±1 in the +4°C +Fe treatment. PSII contribution to photosynthetic protein was 4%±0.4 at T_0 in Bacillariophyta. PSII contribution to the photosynthetic pool remained similar in both the controls, contributing 3%±1 in the *in situ* temperature and 3%±2 in the +4°C treatment at T_f. PSII protein contribution to photosynthetic protein increased in both the iron-amended treatments to 24%±9 in the *in situ* temperature +Fe and 19%±5 in the +4°C +Fe treatments at T_f. ATPase contribution to photosynthetic protein was 33%±6 at T_0 and decreased in both the controls to 22%±6 in the *in situ* temperature and 27%± 12 in the +4°C treatment. Both the iron amended treatments saw increases in contribution

of ATPase to photosynthetic protein, to 40%±7 in the *in situ* temperature +Fe and 42%±4 in the +4°C +Fe treatment at Tf.

In Prymnesiophyceae ATPase was the dominant contributor to the photosynthetic protein pool, starting at 73%±4 at T_0, increasing to 85%±7 in the *in situ* temperature and 85%±2 in the +4°C (Figure 12). ATPase contribution to the photosynthetic protein pool remained similar to T_0 values in both iron treatments, contributing 71%±5 in the *in situ* temperature +Fe and 75%±3 in the +4°C +Fe treatment at T_f. Flavodoxin contribution to the photosynthetic pool was 2%±2 at T_0 and in the *in situ* temperature at T_f. Flavodoxin contribution to the photosynthetic pool was 1%±0.03 in the +4°C, was not detected in the *in situ* temperature and was 0.5%±0.03 in the +4°C +Fe treatment. Plastocyanin was undetected in the +4°C and +4°C +Fe treatments. Plastocyanin contribution to the photosynthetic protein pool was less than 1% at T_0 as well as the *in situ* temperature and less than 2% in the *in situ* temperature +Fe treatment at T_f. PSI contribution to photosynthetic protein was 4%±4 at T_0, remained 4%±0.1 in the *in situ* temperature +Fe treatment and increased slightly to 6%±6 in the +4°C +Fe treatment. PSI contribution to photosynthetic protein decreased in the controls to 1%±0.5 in the *in situ* temperature and 2%±1 in the +4°C. PSII contribution to the photosynthetic protein pool was 13%±3 at T_0, decreased to 9%±5 in the *in situ* temperature and 10%±2 in the +4°C. PSII contribution to the photosynthetic protein pool increased to 18%±5 in the *in situ* temperature +Fe treatment and remained similar to T_0 values with 12%±5 in the +4°C +Fe treatment.

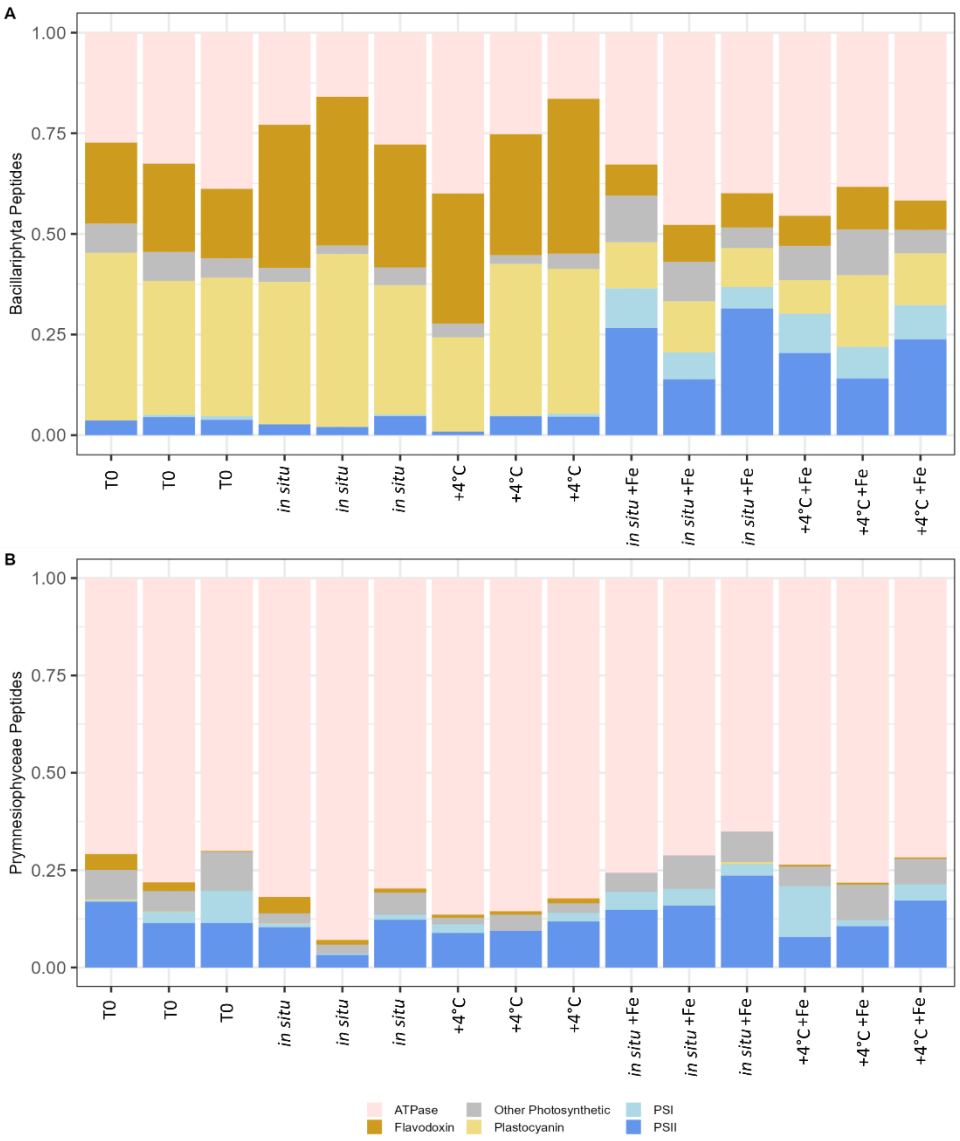

Figure 12. Composition of the light-dependent photosynthetic protein pool in Bacillariophyta and Prymnesiophyceae. Here the total peak area of ATPase, flavodoxin, plastocyanin, PSI, PSII and 'other photosynthetic' peptides were normalized to the total group-specific photosynthetic peptide abundance (Bacillariophyta and Prymnesiophyceae). A-Relative peptide contributions to photosynthetic pool in Bacillariophyta B-Relative peptide contributions to photosynthetic pool in Prymnesiophyceae.

3.9 Flavodoxin and Plastocyanin Protein expression patterns

Flavodoxin and plastocyanin are two classic iron-stress response proteins. We analyzed the expression of each protein normalized to total group-specific protein for Bacillariophyta and Prymnesiophytes throughout the experiment. Here, we were able to assess changes in expression of each of these proteins under both iron-stressed and iron-amended conditions, and then compare the trends observed in our experiment to the trends observed in field samples. In Bacillariophyta, both flavodoxin and plastocyanin were detected in each incubation sample at T_f (Figure 13). Plastocyanin protein expression for Bacillariophyta was highest in the controls at both temperatures. Flavodoxin protein expression was also highest in the controls at both temperatures in Bacillariophyta.

In Prymnesiophyceae flavodoxin was observed in all samples except for one *in situ* temperature +Fe triplicate (Figure 13). Plastocyanin had a paucity of observations in prymnesiophytes, with one observation in a singular *in situ* temperature and *in situ* temperature +Fe sample at T_f. The samples with the greatest flavodoxin protein expression values for prymnesiophytes were found in the controls, at both high and low temperatures.

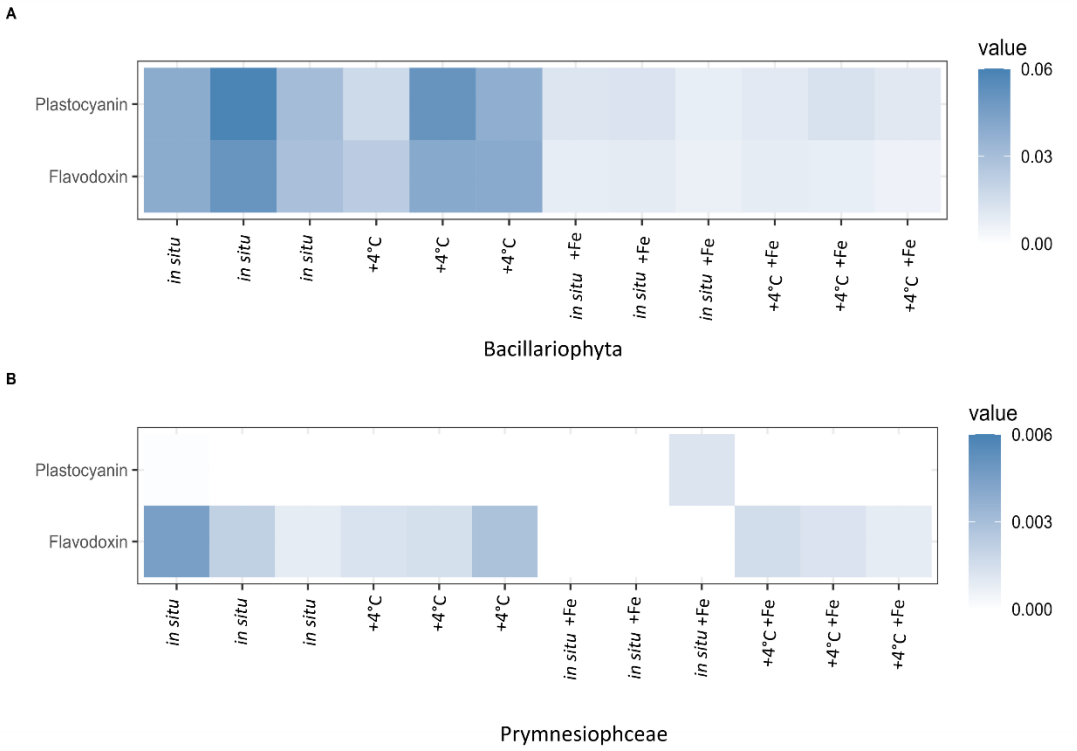

Figure 13. Flavodoxin and plastocyanin peptide expression, normalized to total group peptide abundance in Bacillariophyta and Prymnesiophyceae. A- Flavodoxin and plastocyanin peptide expression in Bacillariophyta B-Flavodoxin and plastocyanin peptide expression in Prymnesiophyceae.

We also examined taxon-normalized flavodoxin and plastocyanin expression in station samples for Bacillariophyta and prymnesiophytes (Figure 14). Both proteins were detected at each depth for each site interrogated in Bacillariophyta. Generally, the greatest plastocyanin protein expression values observed in Bacillariophyta were at the ~25m depth. During initial sampling of the Basin both plastocyanin and flavodoxin expression were higher than was observed in the +Fe treatments. Station 2 reoccupied detected both flavodoxin and plastocyanin in Bacillariophyta although both proteins had much lower values than was observed in the initial sampling of station 2 (Figure 14).

Flavodoxin was detected in prymnesiophytes at all stations and depths except for at 25m at station 2 reoccupied (Figure 14). Stations 2, 4 and 6 saw increased flavodoxin protein expression at the ~25m depth compared to the ~10m samples in prymnesiophytes.

Upon initial sampling of the Basin flavodoxin values were higher than was observed in the +4°C +Fe treatment of the experiment. At station 2 reoccupied flavodoxin was detected at only the 10m sampling depth and was also much lower than the initial observations at station 2. Plastocyanin was not detected in any of the field samples for prymnesiophytes (Figure 14).

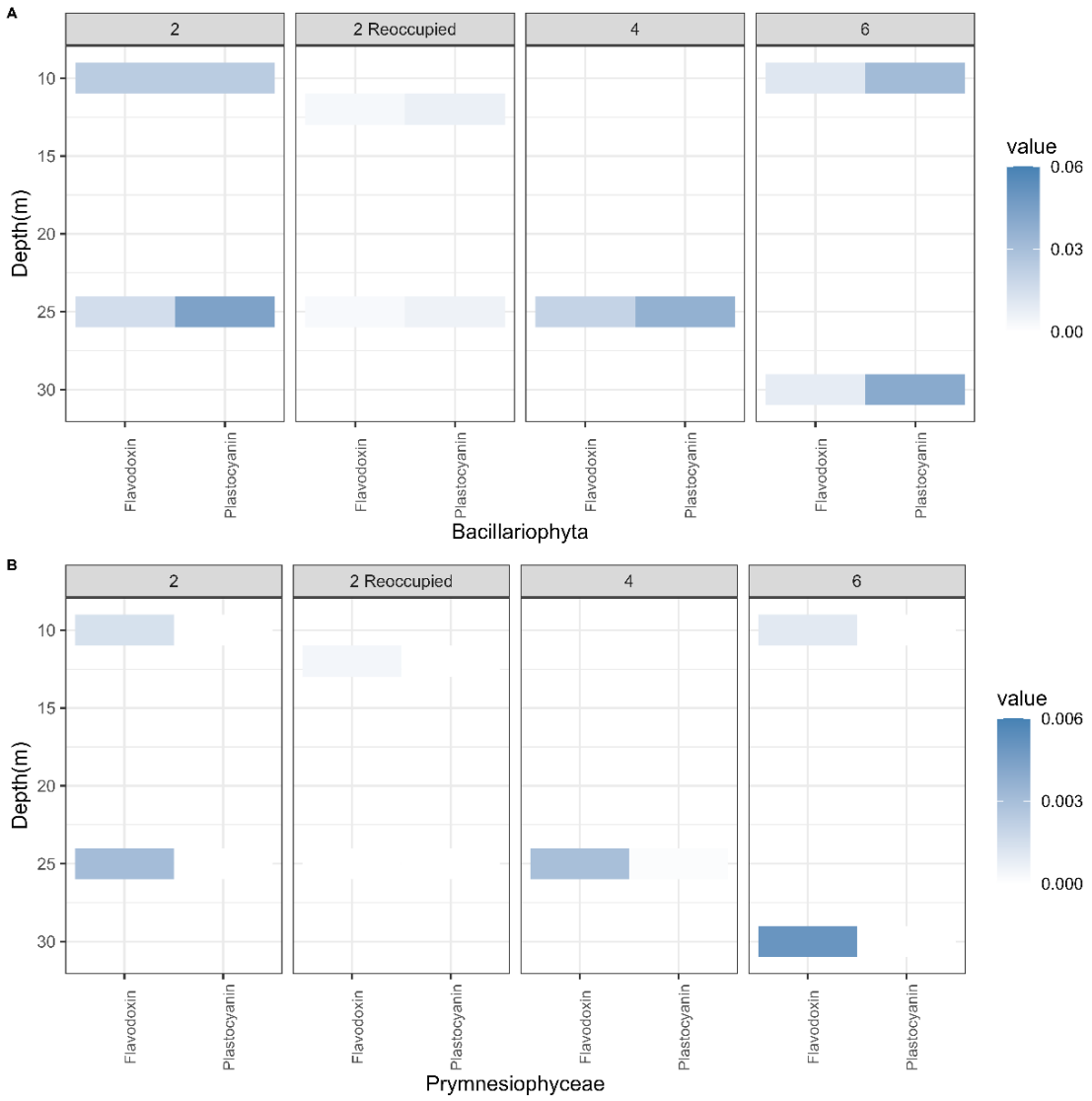

Figure 14. Flavodoxin and plastocyanin peptide expression normalized to total group peptide abundance in Bacillariophyta and Prymnesiophyceae at stations 2, 2 Reoccupied, 4 and 6. A-Flavodoxin and Plastocyanin peptide expression in Bacillariophyta B-Flavodoxin and Plastocyanin peptide expression in Prymnesiophyceae.

Chapter 4: Discussion

4.1 Irminger Basin- Biogeochemical conditions

The prevailing surface nutrient conditions we observed across stations in the Irminger Basin in 2021 were consistent with previous late-summer observations in this region. Past cruises have reported late-summer nitrate concentrations between 2-5μM NO_3^- (Ryan-Keogh et al., 2013; Sanders et al., 2005). Our initial observations of 6-7μM NO_3^- across stations in the Irminger Basin are slightly higher than these previous findings, however, subsequent re-sampling of station 2 roughly a month later found 4.3 μM of surface nitrate, well in agreement with previous observations (Figure 2). Summer surface silicate concentrations have previously been reported between 1-2 μM , and 1-3 μM (Ryan-Keogh et al., 2013) in the Basin, we encountered similar values of 1-2 μM surface silicate across Irminger Basin stations (Figure 4). We encountered extremely low concentrations of dFe 0.05-0.16 nM Fe, which are also consistent with previous observations for this general region (Measures et al., 2008; Nielsdóttir et al., 2009)

4.2 Irminger Basin- Community composition

Community composition was also relatively similar across initial sampling of stations in the Irminger Basin as revealed through both CHEMTAX taxonomic assignment of pigments and metaproteomics. Pigments revealed the photosynthetic community composition to be dominated by C3 flagellates (a grouping of haptophytes and pelagophytes) across field stations and timepoints, with relatively small contributions of diatoms, cryptophytes, chlorophytes and *Synechococcus* to the photosynthetic community (Figure 2). The entire microbial community composition revealed through metaproteomics also showed a consistent makeup across stations, with the majority of protein contribution (50-78%) stemming from ambiguous eukaryotes or other eukaryotes (Figure 5). Bacillariophyta, prymnesiophytes, cryptophytes and dinophytes all respectively contributed less than 5% of protein on average across field samples (Figure 5). Broad community composition remained similar when station 2 was revisited a month after initial sampling, as revealed through both metaproteomics and pigments. However, the composition of Bacillariophyta changed considerably, shifting from *Pseudo-nitzchia* to *Thalassiosira* dominated (Figure 6). The prymnesiophyte composition remained quite

consistent across all stations, with major contributions from *Phaeocystis* and *Chrysochromulina,* although station 6 saw increased relative abundance of *Coccolithu*s (Figure 6). Recent 18S rRNA amplicon-based work has found the major eukaryotic phytoplankton groups in waters surrounding Iceland to be dominated by prymnesiophytes and Bacillariophyta in the summer months; these are congruent with our observations across both methodologies (Cerfonteyn et al., 2023).

The spatial and temporal continuity of surface water nutrients conditions and community composition provides context for our iron-temperature bioassay experiment. Not only are the bioassay results likely to be broadly representative of the Irminger Basin spatially in late-summer of 2021, but to a degree also temporally as late-summer nutrient conditions and broad community composition remained similar a month after initial sampling. These results suggest that our bioassay was representative of the Irminger Basin in the late summer of 2021.

4.3 Iron-limitation in the Irminger Basin

The five-day bioassay experiment manipulating temperature and iron conducted at station 4 revealed clear evidence of iron limitation, and interactive effects of iron and temperature on phytoplankton nutrient drawdown and biomass increase. Iron additions spurred nearly complete drawdown of nitrate after five days in the +4°C +Fe treatment, while a large pool of nitrate (>5µM NO_3^-) remained in the controls (Figure 7). Although the *in situ* temperature +Fe treatment saw increased nitrate drawdown as compared to the controls, it was not the same magnitude as the +4°C +Fe treatment, with an average of ~3 µM NO_3^- remaining at T_f in the *in situ* temperature +Fe treatment. Photophysiology as examined through F_v/F_m values did not see any significant temperature effects but did see significant iron effects ($p<0.001$). F_v/F_m values were extremely similar in the respective Fe conditions, with F_v/F_m values of 0.47 in the *in situ* temperature +Fe and 0.46 in the +4°C +Fe treatment, compared to 0.3 and 0.29 in the controls (Figure 7). Although macronutrients and biomass metrics were not very responsive to iron additions within the first 48h, F_v/F_m values were (Figure 7). One prior iron addition experiment conducted in the Irminger Basin in summer of 2010 saw extremely similar F_v/F_m values in response to +2 nM Fe, and a similar 24-48h lag in biomass response (Ryan-Keough et al., 2013).

Previous work conducted in the Irminger Basin in 2010 found increased nutrient drawdown, increased biomass and increased F_v/F_m values in response to iron additions (Ryan-Keough et al., 2013). In this study, we found similar responses to iron additions, as well as interactive iron and temperature effects on phytoplankton nutrient drawdown and biomass increase. Synergistic iron and temperature effects have previously been found in the Southern Ocean (Rose et al., 2009; Jabre et al. 2021). Here, we show iron and temperature interactively affect phytoplankton in the seasonally-iron limited Irminger Basin.

4.4 Bacillariophyta respond to iron additions in the Irminger Basin

We saw a high degree of community restructuring in response to our bioassay experiment, across all methods used to examine community composition (16S rRNA gene amplicon, CHEMTAX pigment assignments, and metaproteomics). The predominant response to iron additions of community composition was an increase in diatoms (Figure 8). 16S rRNA and pigment data both focused exclusively on the photosynthetic community. The major photosynthetic groups identified across these two methods included diatoms and prymnesiophytes (or C3 flagellates as designated in the pigment grouping). One discrepancy in the observed community composition between these two methods was a high abundance of Cyanophyceae in the 16S rRNA data which was not observed via pigments. A larger filter pore size (0.7 μM) was used to filter samples for pigment collection, which could very plausibly have been too large to capture *Synechococcus*. Upon examining the whole microbial community using the metaproteome, Cyanophyceae did not exceed 2% of the relative protein contribution across experimental samples, compared to prymnesiophytes which ranged from 4-9% of the total microbial community. Across all methods, results showed Bacillariophyta and prymnesiophytes to be among the most abundant photosynthetic community members, with Bacillariophyta responding to iron additions. Temperature did not appear to exert much influence on community structure across methodologies.

We found an extremely uniform composition of Bacillariophyta across the experiment (Figure 9). The dominant Bacillariophyta genus was *Pseudo-nitzschia*, with smaller contributions from *Fragilariopsis*, *Chaetoceros* and *Nitzschia*. The remaining

Bacillariophyta protein was either ambiguous at the class level or belonged to a large diversity of smaller contributors. Bacillariophyta grew from ~3% to 30% of the community composition (Figure 8), however the most abundant Bacillariophyta genera remained consistent across time points and all treatments (Figure 9). A recent paper examining eukaryotic phytoplankton distribution in water masses surrounding Iceland found increased relative abundance of *Pseudo-nitzschia* with higher concentrations of macronutrients, and increased temperatures (Cerfonteyn et al., 2023). *Pseudo-nitzschia* is known to be distinctly flexible in adapting to iron-limitation, and extremely responsive to iron additions. This has been attributed to a suite of molecular responses to iron additions involving both nutrient assimilation and energy acquisition (Cohen et al., 2018; Jabre et al., 2020). Prymnesiophyte composition generally showed more variation across samples, however the two dominant genera, *Phaeocystis* and *Chrysocrhomulina*, remained the same across treatments (Figure 9). *Phaeocystis* has been found to be one of the most abundant prymnesiophytes in surrounding Icelandic waters (Cerfonteyn et al., 2023). *Chrysochromulina* has also been detected in waters surrounding Iceland, although was generally reported to be less abundant than what we observed in the Basin (Cerfonteyn et al., 2023).

4.5 Protein allocation strategies of Bacillariophyta and prymnesiophytes

Diverging investment strategies between phytoplankton taxa in broad functional cellular pools can help explain phytoplankton responses to nutrient stress and impact downstream factors such as preformed nutrients and biogeochemistry (Finkel et al., 2016; Liefer et al., 2019). The ability for different phytoplankton to leverage adjustments in their protein composition in response to abiotic shifts has consequences for biogeochemistry in terms of variable metals requirements and shifts in C:N:P ratios, all of which have consequences for both local, and potentially wide-spread biogeochemistry (Toseland et al., 2013; Peers & Price, 2006; Liefer et al., 2019). In addition, investigating how different phytoplankton groups allocate protein to broad cellular functions can give us insight into the molecular underpinnings driving different growth responses among phytoplankton groups. Consequent changes of dominant community members are liable to impact biogeochemistry through variable nutrient requirements between taxa and differences in sinking rates which may ultimately affect the fate of biological carbon

(Liefer et al., 2019). Thus, understanding both intra and intergroup-specific proteomic responses to shifting abiotic conditions is essential information to track anticipated changes to global nutrient cycling and coarse-grained metaproteomics is one such avenue to interrogate these shifts (McCain et al., 2022). We found elevated protein allocation to ribosomes in Bacillariophyta in response to iron additions ($p<0.001$) (Figure 10). We also found temperature had a statistically significant effect on ribosomal allocation in Bacillariophyta ($p<0.05$), with lower temperatures having the highest ribosomal protein allocation. Although not statistically significant in prymnesiophytes, the highest ribosomal protein allocation values were also found in the *in situ* temperature +Fe treatment (Figure 10). We would expect increased ribosomal investment in fast-growing treatments, as growth requires increased protein synthesis, and therefore ribosomes (Scott et al., 2010). In this case we might expect to observe the highest ribosomal protein allocation in the +4°C +Fe treatment where we also observed the greatest increases in biomass, however, the greatest ribosomal investments were observed in the *in situ* temperature +Fe treatments. These findings may seem incongruous, however, temperature has been shown to modulate the amount of ribosomal protein in diatoms, where ribosomal protein is increased at lower temperatures to compensate for reduced efficiency of protein synthesis (Toseland et al., 2013). This trend has also been revealed through metaproteomics in temperature-iron experiments conducted in the Southern Ocean, where protein allocation to ribosomes was increased at lower temperatures (Jabre et al., in prep).

Light-dependent photosynthetic protein allocation in bacillariophytes remained consistent throughout treatments and in the field (Figures 10, 11). Prymnesiophytes generally had a larger portion of protein allocated to photosynthesis as compared to Bacillariophyta (Figures 10, 11). A previous study examining biovolume of plastids found similar % cellular biovolume of plastids in a diatom and prymensiophyte, although this study did not examine the main genera found in our samples (Uwizeye et al., 2021). Although neither temperature or iron effects were statistically significant in prymnesiophyte photosynthetic protein allocation, both iron and temperature appeared to increase the photosynthetic protein allocation in prymnesiophytes (Figure 10). Bacillariophyta and prymnesiophytes had markedly different protein allocated to rubisco,

with prymnesiophytes having less (Figure 10, 11). We found prymnesiophyte % protein allocated to rubisco comparable to values previously reported in the South Pacific (Losh et al., 2013). Our values for Bacillariophyta % protein allocated to rubisco were higher than those reported in the South Pacific, but comparable to those reported *in situ* in the Southern Ocean during a diatom-dominated bloom, as well as in diatom cultures (Young et al., 2015).

We are in early stages of investigating trends in bulk functional protein allocation, a novel approach to interrogating metaproteomes (McCain et al., 2022). This method has been deployed at various taxonomic grains for photosynthetic and ribosomal protein fractions, in both the Southern Ocean and now the High Latitude North Atlantic. Ribosomal protein fractions in diatoms in the ranged from ~3-20% of protein (Figure 15). The highest values here have been reported in bioassay experiments. Lower values of this range were generally reported at T_{0s} and in controls of these experiments (Jabre et al., in prep), and in field samples (McCain et al., 2022). We generally saw a similar trend in our ribosomal protein fractions in diatoms, our field values ranged from 4-22%, but were often below 10%. Ribosomal fractions in the bioassay experiment ranged from ~5-15%, and the highest values were found in +Fe treatments. Comparing our experimental ribosomal protein fractions with Fe-temperature bioassay experiments conducted in the Southern Ocean, we found similar trends, but generally lower values (McCain et al., 2022; Jabre et al., in prep). Taxonomic variation could contribute to these differences, or different temperature regimes may also contribute to these results. Although the temperature increases in our experiment were +4°C, while temperature was increased +2°C in the Southern Ocean bioassays, our starting temperatures were much higher (9°C), compared to Southern Ocean (~0°C). As previously mentioned, temperature has been shown to exert influence over ribosomal protein investment, this could contribute to the increased ribosomal protein fractions found in Southern Ocean bioassays (Toseland et al., 2013). Southern Ocean values of haptophyte ribosomal mass fraction have ranged from ~11-22%. Again, the highest values were reported in bioassay experiments. Our values in prymnesiophytes ranged from 5-15%. We observed similar patterns of *in situ* temperature +Fe treatments having the highest values, but these were not statistically significant. Diatom photosynthetic mass fractions ranged from ~10-32% across Southern

Ocean observations. Both field and experimental samples showed a high degree of flexibility along this range. We found much less variation in diatom photosynthetic protein investment, spanning 7-14% in the field, and between 9-11% across all treatments. Haptophyte photosynthetic mass fractions have been found to be between 10-30% in the Southern Ocean, with a large degree of spread across both field and experimental samples. We observed prymnesiophyte photosynthetic mass fractions to much more flexible compared to bacillariophytes, with a range of 4-16% in the field, and 8-34% in our bioassay experiment (Figure 15).

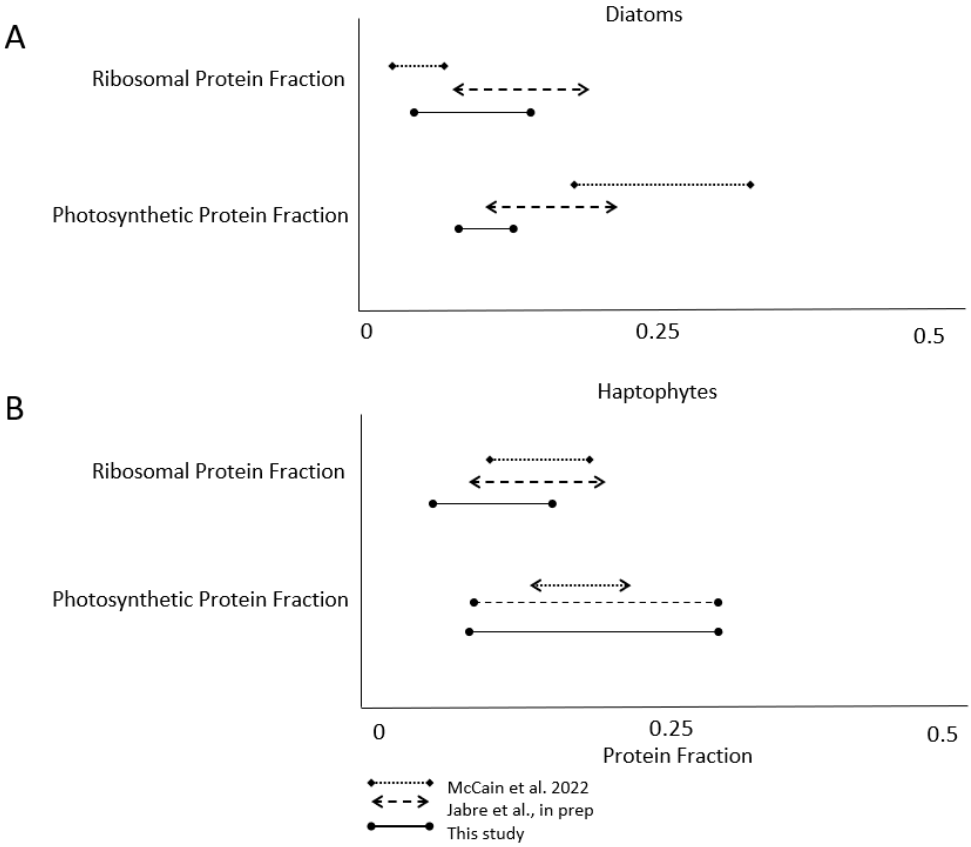

Figure 15. Ribosomal and photosynthetic protein fraction ranges found in diatoms and haptophytes across three studies. A-Diatom ribosomal and photosynthetic protein fractions B-Haptophyte ribosomal and photosynthetic protein fractions. McCain et al., 2022 included environmental samples collected in the Southern Ocean, Jabre et al., in prep included Fe-temperature bioassays conducted in the Southern Ocean, this study included field and bioassay samples in the Irminger Basin.

Several components of light-dependent photosynthesis have Fe requirements, these include electron-carriers such as ferredoxin and cytochrome b_6 as well as photosystems I and II (Raven et al., 1999). Through our bulk analysis of the photosynthetic protein pool, we saw little change in Bacillariophyta allocation to photosynthetic protein (Figure 10). However, upon examination of the relative composition of proteins within the light-dependent photosynthetic pool, such as photosystems I and II, flavodoxin, plastocyanin and chloroplast-associated ATPase we saw distinct restructuring of photosynthetic proteins in Bacillariophyta (Figure 12). Classic iron-stress proteins such as flavodoxin and plastocyanin contributed a much larger fraction of the photosynthetic pool at T_0 and across controls, and both were substantially reduced in iron additions (Figure 12). Meanwhile, iron-containing proteins such as photosystems I and II both showed increased contributions to the photosynthetic pool in +Fe treatments. This same degree of restructuring of photosynthetic protein allocation was not observed in prymnesiophytes. Although not statistically significant, overall protein allocation to the photosynthetic protein pool in prymnesiophytes appeared somewhat responsive to both increased iron and temperatures (Figure 10), and the overall photosynthetic protein investment was higher in prymnesiophytes than Bacillariophyta. In prymnesiophytes, there were minimal changes to the composition of the photosynthetic pool. The vast majority of the photosynthetic protein pool observed in prymnesiophytes belonged to chloroplast-localized ATPase. Plastocyanin was often undetected, and flavodoxin was slightly reduced in +Fe treatments (Figure 12).

4.6 Expression of photosynthetic iron-stress proteins in response to shifting iron and temperature conditions

Flavodoxin and plastocyanin are both non-iron containing proteins that can functionally substitute for iron-containing counterparts. Flavodoxin substitutes for ferredoxin, and plastocyanin substitutes for cytochrome b_6, both have essential roles in light-dependent photosynthetic reactions, and modulation of these proteins have long been linked to iron-stress. Although flavodoxin was identified as a potential iron-stress indicator in the 90s, see LaRoche et al. 1996, its relationship to iron-stress has revealed several nuances in the past 30 years (Karlusich et al., 2014; Wu et al., 2019). Several coastal species of phytoplankton appear to have lost flavodoxin, likely due to their

environment being iron-sufficient, while open-ocean species have generally retained flavodoxin (Karlusich et al., 2014). Some diatoms have been found to have two forms of flavodoxin, with only one form being iron-responsive (Graff Van Creveld et al., 2023; Whitney et al., 2011). Work in the Southern Ocean has found flavodoxin to be both responsive to iron and iron-manganese dynamics in *Phaeocystis* (Wu et al., 2019). A large body of culture experiments and field experiments have often found flavodoxin to be widely responsive to iron-limiting conditions for marine phytoplankton (Behnke et al., 2023; Erdner et al., 1999; LaRoche et al., 1996). Recent transcriptomic analysis has revealed decreased transcription of flavodoxin with iron additions, and rapid increase in ferredoxin on the timescale of one hour in an open-ocean diatom (Behnke et al., 2023). Here, our results find flavodoxin protein expression to be largely regulated by iron availability in both Bacillariophyta and Prymnesiophyceae (Figure 13).

Plastocyanin is a copper-containing electron carrier that can functionally substitute for cytochrome c_6, thereby reducing photosynthetic cellular Fe-requirements (Peers & Price, 2006; Wu et al., 2019). Work in the Southern Ocean has found increased expression of plastocyanin in both haptophytes and diatoms across a temporal gradient of micronutrient stress (McCain et al., 2022). In the Northeastern Pacific, plastocyanin expression has generally been shown to be more highly expressed in iron-limiting conditions for two diatoms as revealed through metatranscriptomics, although this trend diverged at coastal sites (Cohen et al., 2017). Although plastocyanin has often been found to be iron-responsive, this is not always the case. Plastocyanin has been found to be unchanged in diatoms in response to Fe additions in the Southern Ocean, as revealed through metatranscriptomics (Jabre et al., 2021). Culture work examining plastocyanin expression via transcriptomics across iron stressed conditions found plastocyanin to be highly expressed under high iron conditions, and reduced under iron-limiting conditions, behaving similarly to other photosynthetic proteins, and suggesting constitutive expression of plastocyanin in *T. oceanica* (Lommer et al., 2012). Recent work interrogating transcriptional response to alleviation of Fe stress also found transcription of plastocyanin was not iron-responsive (Behnke et al., 2023). Lack of iron-response of plastocyanin expression does not necessarily suggest that it is not being utilized but may indicate that it is permanently substituted in this role, this has particularly been observed

in open-ocean diatoms (Marchetti et al., 2012; Peers & Price, 2006). Furthermore, plastocyanin has also been reported to be temperature-responsive in diatoms, with diverging temperature responses observed in two genera of diatoms (Jabre et al., 2021). Here, we found plastocyanin abundance to be modulated by Fe in Bacillariophyta but were often unable to detect plastocyanin in prymnesiophytes (Figure 13).

Photosystems I and II are essential iron-containing components of photosynthesis. Due to their high iron costs several adaptive strategies have been found amongst phytoplankton to regulate photosystems under iron-limiting conditions. One such mechanisms is the ratio of PSI to PSII, in open vs coastal diatoms, whereby open-ocean diatoms increase their number of PSII which has a lower Fe requirement than PSI (Strzepek & Harrison, 2004). Another iron-conserving mechanism which has been observed in the S.O is increased light-harvesting cross sections of photosystems of S.O phytoplankton (Strzepek et al., 2019). Here, we found Bacillariophyta to dramatically restructure their investments in both PSI and PSII in response to iron conditions. Increases in the contribution of both photosystems to the light-dependent photosynthetic protein pool were observed in +Fe treatments in Bacillariophyta (Figure 12).

4.7 Metaproteomics reveal iron-stress markers in the field

Given that flavodoxin and plastocyanin were responsive to iron conditions in the bioassay we examined their expression across field samples, as potential markers of iron-stress. In Bacillariophyta we saw that initial sampling of the Basin revealed generally higher values of both plastocyanin and flavodoxin as compared to the +Fe treatments in the bioassay, consistent with Fe stress in these field samples (Figure 14). In prymnesiophytes, flavodoxin field values were generally higher than the +Fe treatments, and plastocyanin remained undetected. Station 2 reoccupied represents a deviation from this trend, as flavodoxin values were much reduced in both Bacillariophyta and prymnesiophytes. In Bacillariophyta plastocyanin values were also reduced (Figure 14). Although nitrate was somewhat drawn down at station 2 reoccupied, dFe concentrations remained low (<0.05 nM Fe) at 25m (Figure 2), suggesting that it would be surprising if the plankton were no longer facing iron stress.

We present three possible explanations for this shift in Fe-stress indicator protein expression despite the continued low Fe and high leftover nitrate conditions. First, a pulse of iron could have been delivered to the surface but scavenged by the community before we sampled, satisfying iron demand but being undetectable as a signal in dissolved Fe. This scenario is unlikely for two reasons. Firstly, neither additional aeolian or deep-water fluxes of Fe to the surface would be very likely: resupply of Fe-rich water would not be likely at such strongly stratified time of year, and aeolian flux is limited in this region of the open ocean (Achterberg et al., 2018). Secondly, even if there was an additional Fe source, we know Fe concentrations returned to iron-limiting values, and molecular-responses to iron-limitation are rapid (Behnke et al., 2023). The second scenario could be that the community continued with recycled production, perhaps leveraging both recycled iron and reduced nitrogen sources (Dougdale & Goering, 1967; Zehr et al., 2002). The third scenario is that there were changes in the community composition, with the community transitioning to include species who's flavodoxin and plastocyanin expression are not as tightly regulated by Fe stress status, or who required less flavodoxin and plastocyanin to respond to Fe stress. Although the community composition identified through metaproteomics was consistent at the class level (Figure 5), at the genus level there was a shift in Bacillariophyta, with much less of the community belonging to *Pseudo-nitzschia*, and a larger contribution from *Thalassiosira* (Figure 6). However, we did not see any large changes in prymnesiophyte community composition at the genus level, though a shift at the strain-levels is possible: we would not have resolved it with our approach. We hypothesize that a combination of scenario II and III transpired, where shifting taxonomy may have impacted the expression of iron-stress proteins in Bacillariophyta independent of a change in Fe nutritional status, and the community may also have been able to leverage reduced sources of nitrogen and recycled iron sources to continue production.

Chapter 5: Conclusions

5.1 Overview

Through our bioassay experiment we found clear signs of iron limitation, and interactive iron-temperature effects on phytoplankton growth. Across a suite of methods, we found Bacillariophyta to be responsive to iron additions. Through our metaproteomic analysis we were able to distinguish distinct molecular responses to shifting iron and temperature conditions *in situ*, in our two most abundant phytoplankton groups. We found protein investment to ribosomes to be responsive to Fe and temperatures, however the greatest ribosomal protein investment was observed at lower temperatures, likely to overcome decreased ribosomal efficiency at lower temperatures. Diverging strategies arose between Bacillariophyta and prymensiophyte allocations to photosynthetic protein. Bacillariophytes did not change the proportion of protein allocated to photosynthesis in response to iron or temperature, however there was substantial restructuring of photosynthetic iron-containing proteins and non-iron containing substitutes in response to iron conditions. Prymnesiophytes had an overall greater proportion of photosynthetic protein, but their composition remained more consistent across iron conditions. Leveraging flavodoxin and plastocyanin expression levels in our bioassay allowed us to detect signs of iron-stress in Bacillariophyta and prymnesiophytes across much of the Irminger Basin.

These findings emphasize that taxon-specific molecular strategies are deployed to cope with iron stress. While iron and temperature interactively affect growth, molecular functions are differently impacted by each. Leveraging metaproteomics allowed us to elucidate these nuanced cellular allocation-strategies in response to multiple stressors *in situ*. Interactive Fe-temperature effects on phytoplankton could have a variety of implications for the Basin. Assuming Fe-delivery to the Basin is unchanged, warming waters alone could influence the dynamics of blooms, whereby community biomass and Fe-use efficiency are increased under warmer temperatures. Warming temperatures may also mean shallower winter mixing, and thus decreased Fe delivery to surface waters, this could shorten the new production phase of the bloom cycle and restrict primary production. If Fe availability were to increase in the basin, downstream consequences

could be far-reaching as increased production would likely cause alterations to the amount of preformed nutrients present upon deep-water formation.

5.2 Future Work

Although we were pleased with the performance of the unpaired metatranscriptome database for database searching peptide IDs for these samples, performing this work with a paired database would likely yield increased peptide IDs and thus increase the robustness of this analysis. The high proportion of chloroplast associated ATPase protein particularly in the prymensiophyte photosynthetic pool as compared to Bacillariophyta was a surprising result. However, we did individually BLAST search the most abundant chloroplast associated ATPase peptides and confirmed their annotation was chloroplast-associated through the NCBI database. A future avenue to investigate potential bias for chloroplast associated ATPase protein IDs between Bacillariophyta and Prymnesiophyceae, would be to examine if chloroplast ATPases are more abundant in the metatranscriptome for either group. In addition, while we found further evidence of temperature compensation of ribosomal protein fractions in Bacillariophyta (Toseland et al., 2013, Jabre et al., in prep). To date, our work with protein fractions has been constrained to relatively high latitudes and low temperatures. Expanding the temperature range of our protein fraction work may increase our understanding of how ribosomal protein investment varies with temperatures *in situ.* Culture work conducted across temperature gradients may also improve our understanding here.

Although not included in this thesis, we encountered a range of surface nitrate conditions across the HLNA in the late-summer 2021, with very little surface nitrate observed north of Iceland. Leveraging metaproteomics to track expression of iron-stress proteins along gradients such as these could improve our understanding of the spatial extent of iron stress in the HLNA. This approach, coupled with repeat bioassays, could also serve as a method of tracking the temporal dynamics of iron stress in the Basin.

References

Acevedo-Trejos, E., Brandt, G., Merico, A., & Smith, S. L. (2013). Biogeographical patterns of phytoplankton community size structure in the oceans. Global Ecology and Biogeography, 22(9), 1060–1070. https://doi.org/10.1111/geb.12071

Achterberg, E. P., Moore, C. M., Henson, S. A., Steigenberger, S., Stohl, A., Eckhardt, S., Avendano, L. C., Cassidy, M., Hembury, D., Klar, J. K., Lucas, M. I., Macey, A. I., Marsay, C. M., & Ryan-Keogh, T. J. (2013). Natural iron fertilization by the Eyjafjallajökull volcanic eruption. Geophysical Research Letters, 40(5), 921–926. https://doi.org/10.1002/grl.50221

Achterberg, E. P., Steigenberger, S., Marsay, C. M., LeMoigne, F. A. C., Painter, S. C., Baker, A. R., Connelly, D. P., Moore, C. M., Tagliabue, A., & Tanhua, T. (2018). Iron Biogeochemistry in the High Latitude North Atlantic Ocean. Scientific Reports, 8(1), 1283. https://doi.org/10.1038/s41598-018-19472-1

Alexander, M. A., Scott, J. D., Friedland, K. D., Mills, K. E., Nye, J. A., Pershing, A. J., & Thomas, A. C. (2018). Projected sea surface temperatures over the 21st century: Changes in the mean, variability and extremes for large marine ecosystem regions of Northern Oceans. Elementa: Science of the Anthropocene, 6, 9. https://doi.org/10.1525/elementa.191

Andrew, S. M., Morell, H. T., Strzepek, R. F., Boyd, P. W., & Ellwood, M. J. (2019). Iron availability influences the tolerance of Southern Ocean phytoplankton to warming and elevated irradiance. Frontiers in Marine Science, 6, 681. https://doi.org/10.3389/fmars.2019.00681

Aramaki, T., Blanc-Mathieu, R., Endo, H., Ohkubo, K., Kanehisa, M., Goto, S., & Ogata, H. (2020). KofamKOALA: KEGG Ortholog assignment based on profile HMM and adaptive score threshold. Bioinformatics, 36(7), 2251–2252. https://doi.org/10.1093/bioinformatics/btz859

Beardall, J., Young, E., & Roberts, S. (2001). Approaches for determining phytoplankton nutrient limitation. *Aquatic Sciences*, *63*(1), 44–69. https://doi.org/10.1007/PL00001344

Behnke, J., Cai, Y., Gu, H., & LaRoche, J. (2023). Short-term response to iron resupply in an iron-limited open ocean diatom reveals rapid decay of iron-responsive transcripts. PLOS ONE, 18(1), e0280827. https://doi.org/10.1371/journal.pone.0280827

Boyd, P. W. (2015). Toward quantifying the response of the oceans' biological pump to climate change. Frontiers in Marine Science, 2. https://www.frontiersin.org/articles/10.3389/fmars.2015.00077

Boyd, P. W., Lennartz, S. T., Glover, D. M., & Doney, S. C. (2015). Biological ramifications of climate-change-mediated oceanic multi-stressors. Nature Climate Change, 5(1), 71–79. https://doi.org/10.1038/nclimate2441

Boyd, P. W., Strzepek, R., Fu, F., & Hutchins, D. A. (2010). Environmental control of open-ocean phytoplankton groups: Now and in the future. Limnology and Oceanography, 55(3), 1353–1376. https://doi.org/10.4319/lo.2010.55.3.1353

Capotondi, A., Alexander, M. A., Bond, N. A., Curchitser, E. N., & Scott, J. D. (2012). Enhanced upper ocean stratification with climate change in the CMIP3 models. Journal of Geophysical Research. Oceans, 117(4). https://doi.org/10.1029/2011JC007409

Cerfonteyn, M., Groben, R., Vaulot, D., Guðmundsson, K., Vannier, P., Pérez-Hernández, M. D., & Marteinsson, V. Þ. (2023). The distribution and diversity of eukaryotic phytoplankton in the Icelandic marine environment. Scientific Reports, 13(1), 8519. https://doi.org/10.1038/s41598-023-35537-2

Cohen, N. R., Gong, W., Moran, D. M., McIlvin, M. R., Saito, M. A., & Marchetti, A. (2018). Transcriptomic and proteomic responses of the oceanic diatom *Pseudo-nitzschia granii* to iron limitation. Environmental Microbiology, 20(8), 3109–3126. https://doi.org/10.1111/1462-2920.14386

Cohen, N. R., Ellis, K. A., Lampe, R. H., McNair, H., Twining, B. S., Maldonado, M. T., Brzezinski, M. A., Kuzminov, F. I., Thamatrakoln, K., Till, C. P., Bruland, K. W., Sunda, W. G., Bargu, S., & Marchetti, A. (2017). Diatom Transcriptional and Physiological Responses to Changes in Iron Bioavailability across Ocean Provinces. *Frontiers in Marine Science*, *4*. https://www.frontiersin.org/articles/10.3389/fmars.2017.00360

Cullen, J. J. (1991). Hypotheses to explain high-nutrient conditions in the open sea. Limnology and Oceanography, 36(8), 1578–1599.

De Baar, H. J. W., Timmermans, K. R., Laan, P., De Porto, H. H., Ober, S., Blom, J. J., Bakker, M. C., Schilling, J., Sarthou, G., Smit, M. G., & Klunder, M. (2008). Titan: A new facility for ultraclean sampling of trace elements and isotopes in the deep oceans in the international Geotraces program. Marine Chemistry, 111(1–2), 4–21. https://doi.org/10.1016/j.marchem.2007.07.009

Decelle, J., Romac, S., Stern, R. F., Bendif, E. M., Zingone, A., Audic, S., Guiry, M. D., Guillou, L., Tessier, D., Le Gall, F., Gourvil, P., Dos Santos, A. L., Probert, I., Vaulot, D., De Vargas, C., & Christen, R. (2015). PhytoREF: A reference database of the plastidial 16S rRNA gene of photosynthetic eukaryotes with curated taxonomy. Molecular Ecology Resources, 15(6), 1435–1445. https://doi.org/10.1111/1755-0998.12401

DeVries, T., Primeau, F., & Deutsch, C. (2012). The sequestration efficiency of the biological pump. Geophysical Research Letters, 39(13), n/a-n/a. https://doi.org/10.1029/2012GL051963

Dickson, B., Meincke, J., & Rhines, P. (2008). Arctic–Subarctic Ocean fluxes: defining the role of the Northern Seas in climate. In R. R. Dickson, J. Meincke, & P. Rhines (Eds.), Arctic–Subarctic Ocean Fluxes: Defining the Role of the Northern Seas in Climate (pp. 1–13). Springer Netherlands. https://doi.org/10.1007/978-1-4020-6774-7_1

Dugdale, R. C., & Goering, J. J. (1967). Uptake of new and regenerated forms of nitrogen in primary productivity. Limnology and Oceanography, *12*(2), 196–206. https://doi.org/10.4319/lo.1967.12.2.0196

Elias, J. E., & Gygi, S. P. (2007). Target-decoy search strategy for increased confidence in large-scale protein identifications by mass spectrometry. Nature Methods, 4(3), 207–214. https://doi.org/10.1038/nmeth1019

Eppley, R. W., & Peterson, B. J. (1979). Particulate organic matter flux and planktonic new production in the deep ocean. Nature, 282(5740), 677–680. https://doi.org/10.1038/282677a0

Erdner, D., Price, NM., Doucette, G., Peleato, ML., & Anderson, DM. (1999). Characterization of ferredoxin and flavodoxin as markers of iron limitation in marine phytoplankton. Marine Ecology Progress Series, 184, 43–53. https://doi.org/10.3354/meps184043

Eren, A. M., Kiefl, E., Shaiber, A., Veseli, I., Miller, S. E., Schechter, M. S., Fink, I., Pan, J. N., Yousef, M., Fogarty, E. C., Trigodet, F., Watson, A. R., Esen, Ö. C., Moore, R. M., Clayssen, Q., Lee, M. D., Kivenson, V., Graham, E. D., Merrill, B. D., … Willis, A. D. (2021). Community-led, integrated, reproducible multi-omics with anvi'o. Nature Microbiology, 6(1), Article 1. https://doi.org/10.1038/s41564-020-00834-3

Finkel, Z. V., Beardall, J., Flynn, K. J., Quigg, A., Rees, T. A. V., & Raven, J. A. (2010). Phytoplankton in a changing world: Cell size and elemental stoichiometry. Journal of Plankton Research, *32*(1), 119–137. https://doi.org/10.1093/plankt/fbp09

Gerringa, L. J. A., Alderkamp, A.-C., Van Dijken, G., Laan, P., Middag, R., & Arrigo, K. R. (2020). Dissolved trace metals in the Ross Sea. Frontiers in Marine Science, 7, 577098. https://doi.org/10.3389/fmars.2020.577098

Grabherr, M. G., Haas, B. J., Yassour, M., Levin, J. Z., Thompson, D. A., Amit, I., Adiconis, X., Fan, L., Raychowdhury, R., Zeng, Q., Chen, Z., Mauceli, E., Hacohen, N., Gnirke, A., Rhind, N., di Palma, F., Birren, B. W., Nusbaum, C., Lindblad-Toh, K., … Regev, A. (2011). Trinity: Reconstructing a full-length transcriptome without a genome from RNA-Seq data. Nature Biotechnology, 29(7), 644–652. https://doi.org/10.1038/nbt.1883

Graff Van Creveld, S., Coesel, S. N., Blaskowski, S., Groussman, R. D., Schatz, M. J., & Armbrust, E. V. (2023). Divergent functions of two clades of flavodoxin in diatoms mitigate oxidative stress and iron limitation. ELife, 12, e84392. https://doi.org/10.7554/eLife.84392

Hyatt, D., Chen, G.-L., LoCascio, P. F., Land, M. L., Larimer, F. W., & Hauser, L. J. (2010). Prodigal: Prokaryotic gene recognition and translation initiation site identification. BMC Bioinformatics, 11(1), 119. https://doi.org/10.1186/1471-2105-11-119

Jabre, L., Allen, A. E., McCain, J. S. P., McCrow, J. P., Tenenbaum, N., Spackeen, J. L., Sipler, R. E., Green, B. R., Bronk, D. A., Hutchins, D. A., & Bertrand, E. M. (2020). Molecular underpinnings and biogeochemical consequences of enhanced diatom growth in a warming Southern Ocean. Ecology. https://doi.org/10.1101/2020.07.01.177865

Jabre, L., Allen, A. E., McCain, J. S. P., McCrow, J. P., Tenenbaum, N., Spackeen, J. L., Sipler, R. E., Green, B. R., Bronk, D. A., Hutchins, D. A., & Bertrand, E. M. (2021). Molecular underpinnings and biogeochemical consequences of enhanced diatom growth in a warming Southern Ocean. Proceedings of the National Academy of Sciences, 118(30), e2107238118. https://doi.org/10.1073/pnas.2107238118

Jabre, L., van Manen, M., Eich, C., Van de Poll, W., Rowland, E., Brussard, C., Middag, R., Bertrand, E. (2023). Metaproteomic insights into elemental stoichiometry in a changing Southern Ocean. Manuscript in preparation.

Jabre, L., & Bertrand, E. M. (2020). Interactive effects of iron and temperature on the growth of *Fragilariopsis cylindrus*. Limnology and Oceanography Letters, 5(5), 363–370. https://doi.org/10.1002/lol2.10158

Kanehisa, M., & Goto, S. (2000). KEGG: Kyoto encyclopedia of genes and genomes. Nucleic Acids Research, 28(1), 27–30. https://doi.org/10.1093/nar/28.1.27

Karlusich, J. J., Lodeyro, A. F., & Carrillo, N. (2014). The long goodbye: The rise and fall of flavodoxin during plant evolution. Journal of Experimental Botany, 65(18), 5161–5178. https://doi.org/10.1093/jxb/eru273

Keeling, P. J., Burki, F., Wilcox, H. M., Allam, B., Allen, E. E., Amaral-Zettler, L. A., Armbrust, E. V., Archibald, J. M., Bharti, A. K., Bell, C. J., Beszteri, B., Bidle, K. D., Cameron, C. T., Campbell, L., Caron, D. A., Cattolico, R. A., Collier, J. L., Coyne, K., Davy, S. K., … Worden, A. Z. (2014). The marine microbial eukaryote transcriptome sequencing project (MMETSP): illuminating the functional diversity of eukaryotic life in the oceans through transcriptome sequencing. PLOS Biology, 12(6), e1001889. https://doi.org/10.1371/journal.pbio.1001889

Klemetsen, T., Raknes, I. A., Fu, J., Agafonov, A., Balasundaram, S. V., Tartari, G., Robertsen, E., & Willassen, N. P. (2018). The MAR databases: Development and implementation of databases specific for marine metagenomics. Nucleic Acids Research, 46, D692–D699. https://doi.org/10.1093/nar/gkx1036

Kim, S., & Pevzner, P. A. (2014). MS-GF+ makes progress towards a universal database search tool for proteomics. Nature Communications, 5(1), 5277. https://doi.org/10.1038/ncomms6277

Krinos, A. I., Hu, S. K., Cohen, N. R., & Alexander, H. (2021). EUKulele: Taxonomic annotation of the unsung eukaryotic microbes. Journal of Open Source Software, 6(57), 2817. https://doi.org/10.21105/joss.02817

Liefer, J. D., Garg, A., Fyfe, M. H., Irwin, A. J., Benner, I., Brown, C. M., Follows, M. J., Omta, A. W., & Finkel, Z. V. (2019). The Macromolecular Basis of Phytoplankton C:N:P Under Nitrogen Starvation. Frontiers in Microbiology, 10. https://www.frontiersin.org/articles/10.3389/fmicb.2019.0076

Langmead, B., & Salzberg, S. L. (2012). Fast gapped-read alignment with Bowtie 2. Nature Methods, 9(4), 357–359. https://doi.org/10.1038/nmeth.1923

LaRoche, J., Boyd, P. W., McKay, R. M. L., & Geider, R. J. (1996). Flavodoxin as an in situ marker for iron stress in phytoplankton. Nature, 382(6594), 802–805. https://doi.org/10.1038/382802a0

Logemann, K., Ólafsson, J., Snorrason, Á., Valdimarsson, H., & Marteinsdóttir, G. (2013). The circulation of Icelandic waters – a modelling study. Ocean Sci, 9, 931-955. https//doi.org/:10.5194/os-9-931-2013

Lommer, M., Specht, M., Roy, A.-S., Kraemer, L., Andreson, R., Gutowska, M. A., Wolf, J., Bergner, S. V., Schilhabel, M. B., Klostermeier, U. C., Beiko, R. G., Rosenstiel, P., Hippler, M., & LaRoche, J. (2012). Genome and low-iron response of an oceanic diatom adapted to chronic iron limitation. *Genome Biology*, *13*(7), R66. https://doi.org/10.1186/gb-2012-13-7-r66

Losh, J. L., Young, J. N., & Morel, F. M. M. (2013). Rubisco is a small fraction of total protein in marine phytoplankton. New Phytologist, 198(1), 52–58. https://doi.org/10.1111/nph.12143

Mackey, M., Mackey, D., Higgins, H., & Wright, S. (1996). CHEMTAX - a program for estimating class abundances from chemical markers: application to HPLC measurements of phytoplankton. Marine Ecology Progress Series, 144, 265–283. https://doi.org/10.3354/meps144265

Marinov, I., Gnanadesikan, A., Sarmiento, J. L., Toggweiler, J. R., Follows, M., & Mignone, B. K. (2008). Impact of oceanic circulation on biological carbon storage in the ocean and atmospheric p CO 2. Global Biogeochemical Cycles, 22(3). https://doi.org/10.1029/2007GB002958

McCain, J. S. P., Allen, A. E., & Bertrand, E. M. (2022). Proteomic traits vary across taxa in a coastal Antarctic phytoplankton bloom. The ISME Journal, 16(2), 569–579. https://doi.org/10.1038/s41396-021-01084-9

McCain, J. S. P., & Bertrand, E. M. (2019). Prediction and consequences of cofragmentation in metaproteomics. Journal of Proteome Research, 18(10), 3555–3566. https://doi.org/10.1021/acs.jproteome.9b00144

Measures, C. I., Landing, W. M., Brown, M. T., & Buck, C. S. (2008). High-resolution Al and Fe data from the Atlantic Ocean CLIVAR-CO2 Repeat Hydrography A16N transect: Extensive linkages between atmospheric dust and upper ocean geochemistry. Global Biogeochemical Cycles, 22(1). https://doi.org/10.1029/2007GB003042

Mistry, J., Chuguransky, S., Williams, L., Qureshi, M., Salazar, G. A., Sonnhammer, E. L. L., Tosatto, S. C. E., Paladin, L., Raj, S., Richardson, L. J., Finn, R. D., & Bateman, A. (2021). Pfam: The protein families database in 2021. Nucleic Acids Research, 49(D1), D412–D419. https://doi.org/10.1093/nar/gkaa913

Moore, C. M., Lucas, M. I., Sanders, R., & Davidson, R. (2005). Basin-scale variability of phytoplankton bio-optical characteristics in relation to bloom state and community structure in the Northeast Atlantic. Deep Sea Research Part I: Oceanographic Research Papers, 52(3), 401–419. https://doi.org/10.1016/j.dsr.2004.09.003

Moore, C. M., Mills, M. M., Arrigo, K. R., Berman-Frank, I., Bopp, L., Boyd, P. W., Galbraith, E. D., Geider, R. J., Guieu, C., Jaccard, S. L., Jickells, T. D., La Roche, J., Lenton, T. M., Mahowald, N. M., Marañón, E., Marinov, I., Moore, J. K., Nakatsuka, T., Oschlies, A., … Ulloa, O. (2013). Processes and patterns of oceanic nutrient limitation. Nature Geoscience, 6(9), 701–710. https://doi.org/10.1038/ngeo1765

Nielsdóttir, M. C., Moore, C. M., Sanders, R., Hinz, D. J., & Achterberg, E. P. (2009). Iron limitation of the postbloom phytoplankton communities in the Iceland Basin. Global Biogeochemical Cycles, 23(3). https://doi.org/10.1029/2008GB003410

Oziel, L., Baudena, A., Ardyna, M., Massicotte, P., Randelhoff, A., Sallée, J.-B., Ingvaldsen, R. B., Devred, E., & Babin, M. (2020). Faster Atlantic currents drive poleward expansion of temperate phytoplankton in the Arctic Ocean. Nature Communications, 11(1), 1705. https://doi.org/10.1038/s41467-020-15485-5

Parada, A. E., Needham, D. M., & Fuhrman, J. A. (2016). Every base matters: Assessing small subunit rRNA primers for marine microbiomes with mock communities, time series and global field samples. Environmental Microbiology, *18*(5), 1403–1414. https://doi.org/10.1111/1462-2920.13023

Peers, G., & Price, N. M. (2006). Copper-containing plastocyanin used for electron transport by an oceanic diatom. *Nature*, *441*(7091), 341–344. https://doi.org/10.1038/nature04630

Rapp, I., Guzman, M., Desai, D., Rowland, E., LaRoche, J., Bertrand, E. (2023). Molecular physiology of multiple nutrient limitation in the North West Atlantic near Greenland. Manuscript in preparation.

Raven, J. A. (1988). The iron and molybdenum use efficiencies of plant growth with different energy, carbon and nitrogen sources. New Phytologist, 109(3), 279–287. https://doi.org/10.1111/j.1469-8137.1988.tb04196.x

Raven, J. A., Evans, M. C. W., & Korb, R. E. (1999). The role of trace metals in photosynthetic electron transport in O2-evolving organisms. Photosynthesis Research, 60, 111-149.

Raven, J. A., & Geider, R. J. (1988). Temperature and algal growth. New Phytologist, 110(4), 441–461. https://doi.org/10.1111/j.1469-8137.1988.tb00282.x

Rijkenberg, M. J. A., De Baar, H. J. W., Bakker, K., Gerringa, L. J. A., Keijzer, E., Laan, M., Laan, P., Middag, R., Ober, S., Van Ooijen, J., Ossebaar, S., Van Weerlee, E. M., & Smit, M. G. (2015). "PRISTINE", a new high volume sampler for ultraclean sampling of trace metals and isotopes. Marine Chemistry, 177, 501–509. https://doi.org/10.1016/j.marchem.2015.07.001

Robicheau, B. M., Tolman, J., Bertrand, E. M., & LaRoche, J. (2022). Highly-resolved interannual phytoplankton community dynamics of the coastal Northwest Atlantic. ISME Communications, 2(1), Article 1. https://doi.org/10.1038/s43705-022-00119-2

Rose, J. M., Feng, Y., DiTullio, G. R., Dunbar, R. B., Hare, C. E., Lee, P. A., Lohan, M., Long, M., W. O. Smith Jr., Sohst, B., Tozzi, S., Zhang, Y., & Hutchins, D. A. (2009). Synergistic effects of iron and temperature on Antarctic phytoplankton and microzooplankton assemblages. Biogeosciences, 6(12), 3131–3147. https://doi.org/10.5194/bg-6-3131-2009

Röst, H. L., Sachsenberg, T., Aiche, S., Bielow, C., Weisser, H., Aicheler, F., Andreotti, S., Ehrlich, H.-C., Gutenbrunner, P., Kenar, E., Liang, X., Nahnsen, S., Nilse, L., Pfeuffer, J., Rosenberger, G., Rurik, M., Schmitt, U., Veit, J., Walzer, M., … Kohlbacher, O. (2016). OpenMS: A flexible open-source software platform for mass spectrometry data analysis. Nature Methods, 13(9), 741–748. https://doi.org/10.1038/nmeth.3959

Rudels, B., Björk, G., Nilsson, J., Winsor, P., Lake, I., & Nohr, C. (2005). The interaction between waters from the Arctic Ocean and the Nordic Seas north of Fram Strait and along the East Greenland Current: Results from the Arctic Ocean-02 Oden expedition. Journal of Marine Systems, 55(1–2), 1–30. https://doi.org/10.1016/j.jmarsys.2004.06.008

Ryan-Keogh, T. J., Macey, A. I., Nielsdóttir, M. C., Lucas, M. I., Steigenberger, S. S., Stinchcombe, M. C., Achterberg, E. P., Bibby, T. S., & Moore, C. M. (2013). Spatial and temporal development of phytoplankton iron stress in relation to bloom dynamics in the high-latitude North Atlantic Ocean. Limnology and Oceanography, 58(2), 533–545. https://doi.org/10.4319/lo.2013.58.2.0533

Saito, M. A., Bertrand, E. M., Duffy, M. E., Gaylord, D. A., Held, N. A., Hervey, W. J., Hettich, R. L., Jagtap, P. D., Janech, M. G., Kinkade, D. B., Leary, D. H., McIlvin, M. R., Moore, E. K., Morris, R. M., Neely, B. A., Nunn, B. L., Saunders, J. K., Shepherd, A. I., Symmonds, N. I., & Walsh, D. A. (2019). Progress and Challenges in Ocean Metaproteomics and Proposed Best Practices for Data Sharing. Journal of Proteome Research, 18(4), 1461–1476. https://doi.org/10.1021/acs.jproteome.8b00761

Saito, M. A., Goepfert, T. J., & Ritt, J. T. (2008). Some thoughts on the concept of colimitation: Three definitions and the importance of bioavailability. Limnology and Oceanography, 53(1), 276–290. https://doi.org/10.4319/lo.2008.53.1.0276

Sanders, R., Brown, L., Henson, S., & Lucas, M. (2005). New production in the Irminger Basin during 2002. Journal of Marine Systems, 55(3–4), 291–310. https://doi.org/10.1016/j.jmarsys.2004.09.002

Schoffman, H., Lis, H., Shaked, Y., & Keren, N. (2016). Iron–Nutrient Interactions within Phytoplankton. Frontiers in Plant Science, 7. https://doi.org/10.3389/fpls.2016.01223

Scott, M., Gunderson, C. W., Mateescu, E. M., Zhang, Z., & Hwa, T. (2010). Interdependence of cell growth and gene expression: origins and consequences. Science, 330(6007), 1099–1102. https://doi.org/10.1126/science.1192588

Spackeen, J. L., Bronk, D. A., Sipler, R. E., Bertrand, E. M., Hutchins, D. A., & Allen, A. E. (2018). Stoichiometric N:P ratios, temperature, and iron impact carbon and nitrogen uptake by Ross Sea microbial communities. Journal of Geophysical Research: Biogeosciences, 123(9), 2955–2975. https://doi.org/10.1029/2017JG004316

Strzepek, R. F., Boyd, P. W., & Sunda, W. G. (2019). Photosynthetic adaptation to low iron, light, and temperature in Southern Ocean phytoplankton. Proceedings of the National Academy of Sciences, 116(10), 4388–4393. https://doi.org/10.1073/pnas.1810886116

Strzepek, R. F., & Harrison, P. J. (2004). Photosynthetic architecture differs in coastal and oceanic diatoms. Nature, 431(7009), 689–692. https://doi.org/10.1038/nature02954

Sverdrup, H. U. (1953). On Conditions for the Vernal Blooming of Phytoplankton. ICES Journal of Marine Science, 18(3), 287–295. https://doi.org/10.1093/icesjms/18.3.287

Tatusov, R. L., Koonin, E. V., & Lipman, D. J. (1997). A genomic perspective on protein families. Science, 278(5338), 631–637.

Tonnard, M., Planquette, H., Bowie, A. R., Van Der Merwe, P., Gallinari, M., Desprez De Gésincourt, F., Germain, Y., Gourain, A., Benetti, M., Reverdin, G., Tréguer, P., Boutorh, J., Cheize, M., Lacan, F., Menzel Barraqueta, J.-L., Pereira-Contreira, L., Shelley, R., Lherminier, P., & Sarthou, G. (2020). Dissolved iron in the North Atlantic Ocean and Labrador Sea along the GEOVIDE section (GEOTRACES section GA01). Biogeosciences, 17(4), 917–943. https://doi.org/10.5194/bg-17-917-2020

Toseland, A., Daines, S. J., Clark, J. R., Kirkham, A., Strauss, J., Uhlig, C., Lenton, T. M., Valentin, K., Pearson, G. A., Moulton, V., & Mock, T. (2013). The impact of temperature on marine phytoplankton resource allocation and metabolism. Nature Climate Change, 3(11), 979–984. https://doi.org/10.1038/nclimate1989

Toulza, E., Tagliabue, A., Blain, S., & Piganeau, G. (2012). Analysis of the global ocean sampling (GOS) project for trends in iron uptake by surface ocean microbes. PLoS ONE, 7(2), e30931. https://doi.org/10.1371/journal.pone.0030931

Uwizeye, C., Decelle, J., Jouneau, P.-H., Flori, S., Gallet, B., Keck, J.-B., Bo, D. D., Moriscot, C., Seydoux, C., Chevalier, F., Schieber, N. L., Templin, R., Allorent, G., Courtois, F., Curien, G., Schwab, Y., Schoehn, G., Zeeman, S. C., Falconet, D., & Finazzi, G. (2021). Morphological bases of phytoplankton energy management and physiological responses unveiled by 3D subcellular imaging. Nature Communications, 12(1), Article 1. https://doi.org/10.1038/s41467-021-21314-0

Van de Poll, W. H., Kulk, G., Timmermans, K. R., Brussaard, C. P. D., van der Woerd, H. J., Kehoe, M. J., Mojica, K. D. A., Visser, R. J. W., Rozema, P. D., & Buma, A. G. J. (2013). Phytoplankton chlorophyll a; biomass, composition, and productivity along a temperature and stratification gradient in the northeast Atlantic Ocean. Biogeosciences, 10(6), 4227–4240. https://doi.org/10.5194/bg-10-4227-2013

Van Heukelem, L., & Thomas, C. S. (2001). Computer-assisted high-performance liquid chromatography method development with applications to the isolation and analysis of phytoplankton pigments. Journal of Chromatography A, 910(1), 31–49. https://doi.org/10.1016/S0378-4347(00)00603-4

van Leeuwe, M. A., Villerius, L. A., Roggeveld, J., Visser, R. J. W., & Stefels, J. (2006). An optimized method for automated analysis of algal pigments by HPLC. Marine Chemistry, 102(3), 267–275. https://doi.org/10.1016/j.marchem.2006.05.003

Verardo, D. J., Froelich, P. N., & McIntyre, A. (1990). Determination of organic carbon and nitrogen in marine sediments using the Carlo Erba NA-1500 analyzer. Deep Sea Research Part A. Oceanographic Research Papers, 37(1), 157–165. https://doi.org/10.1016/0198-0149(90)90034-S

Vihtakari, M (2023). ggOceanMaps: Plot data on oceanographic maps using ‘ggplot2’. R package version 2.0.3 <https://mikkovihtakari.github.io/ggOceanMaps/>.

Weisser, H., & Choudhary, J. S. (2017). Targeted feature detection for data-dependent shotgun proteomics. Journal of Proteome Research, 16(8), 2964–2974. https://doi.org/10.1021/acs.jproteome.7b00248

White, P. (2023). Resolving the impact of glacier-derived nutrients on marine phytoplankton. Master’s thesis, University of Alberta. Manuscript in preparation.

Whitney, L. P., Lins, J. J., Hughes, M. P., Wells, M. L., Chappell, P. D., & Jenkins, B. D. (2011). Characterization of putative iron responsive genes as species-specific indicators of iron stress in Thalassiosiroid diatoms. Frontiers in Microbiology, 2. https://doi.org/10.3389/fmicb.2011.00234

Wilmes, P., & Bond, P. 2004. The application of two-dimensional polyacrylamide gel electrophoresis and downstream analyses to a mixed community of prokaryotic microorganisms. Environmental microbiology, 6(9), 911-20. doi:10.1111/j.1462-2920.2004.00687.x

Wu, M., McCain, J. S. P., Rowland, E., Middag, R., Sandgren, M., Allen, A. E., & Bertrand, E. M. (2019). Manganese and iron deficiency in Southern Ocean *Phaeocystis antarctica* populations revealed through taxon-specific protein indicators. Nature Communications, 10(1), 3582. https://doi.org/10.1038/s41467-019-11426-z

Yilmaz, P., Parfrey, L. W., Yarza, P., Gerken, J., Pruesse, E., Quast, C., Schweer, T., Peplies, J., Ludwig, W., & Glöckner, F. O. (2014). The SILVA and "All-species Living Tree Project (LTP)" taxonomic frameworks. Nucleic Acids Research, 42(D1), D643–D648. https://doi.org/10.1093/nar/gkt1209

Young, J. N., Goldman, J. A. L., Kranz, S. A., Tortell, P. D., & Morel, F. M. M. (2015). Slow carboxylation of Rubisco constrains the rate of carbon fixation during Antarctic phytoplankton blooms. New Phytologist, 205(1), 172–181. https://doi.org/10.1111/nph.1302

Zehr, J. P., & Ward, B. B. (2002). Nitrogen Cycling in the Ocean: New Perspectives on Processes and Paradigms. Applied and Environmental Microbiology, 68(3), 1015–1024. https://doi.org/10.1128/AEM.68.3.1015-1024.200

Appendix A: Supplemental Information

S1. MetalGate Station coordinates.

Station	Latitude	Longitude
2	N 62° 10' 12.22"	W 29° 49' 46.524"
4	N 60° 18' 38.185"	W 36° 3' 12.672"
6	N 60° 0' 0.14"	W 40° 10' 12.479"
7	N 61° 36' 0.295"	W 38° 59' 58.351"
2 Reoccupied	N 62° 10' 15.719"	W 29° 49' 45.03"

S2. Two-way ANOVA results for biogeochemical response to an Fe-temperature bioassay experiment.

	in situ	+4°C	*in situ* +Fe	+4°C +Fe	Main effect temperature	Main effect iron	Iron-temperature interactive effect
F_v/F_m	0.30(0.05)	0.29(0.01)	0.47(0.04)	0.46(0.00)	ns	***	ns
NO_3^-	6.43(0.46)	5.50(0.23)	2.73(0.96)	0.06(0.01)	***	***	*
$PO_4^{3`}$	0.47(0.03)	0.42(0.01)	0.25(0.07)	0.08(0.01)	**	***	*
Si	1.56(0.08)	1.28(0.03)	0.69(0.23)	0.10(0.06)	***	***	ns
Chl-a	0.46(0.2)	0.7(0.02)	2.6(0.4)	4.7(0.8)	**	***	**

Values are means and SD are shown in brackets (n=3)

(*p<0.05, **p<0.01, ***p<0.001)

S3. The total number of group-specific peptides identified for Bacillariophyta and Prymnesiophyceae, and the number of group-specific peptides identified for specific proteins and protein pools across the dataset.

	All	Ribosomal	Photosynthetic	Rubisco	Flavodoxin	Plastocyanin
Bacillariophyta	4954	588	270	46	33	14
Prymnesiophyceae	4119	468	397	67	23	9

S4. Two-way ANOVA results for protein fraction response to an Fe-temperature bioassay experiment in Bacillariophyta.

Bacillariophyta	*in situ*	+4°C	*in situ* +Fe	+4°C +Fe	Temperature main effect	Iron main effect	Iron-temperature interactive effect
Ribosomal Mass Fraction	0.09(0.01)	0.07(0.01)	0.13(0.02)	0.09(0.01)	*	**	ns
Photosynthetic Mass Fraction	0.11(0.02)	0.10(0.02)	0.10(0.01)	0.09(0.02)	ns	ns	ns
Rubisco Mass Fraction	0.08(0.03)	0.10(0.04)	0.16(0.09)	0.19I(0.09)	ns	ns	ns

Values are means and SD are shown in brackets (n=3)

(*p<0.05, **p<0.01, ***p<0.001)

S5. Two-way ANOVA results for protein fraction response to an Fe-temperature bioassay experiment in Prymnesiophyceae.

Prymnesiophyte	*in situ*	+4°C	*in situ* +Fe	+4°C +Fe	Temperature main effect	Main effect iron	Iron-temperature interactive effect
Ribosomal Mass Fraction	0.06(0.03)	0.10(0.04)	0.12(0.04)	0.10(0.02)	ns	ns	ns
Photosynthetic Mass Fraction	0.12(0.05)	0.19(0.03)	0.19(0.09)	0.27(0.07)	ns	ns	ns
Rubisco Mass Fraction	0.02(0.01)	0.05(0.03)	0.03(0.02)	0.06(0.02)	*	ns	ns

Values are means and SD are shown in brackets (n=3)

(*p<0.05, **p<0.01, ***p<0.001)

S6. The number of peptides identified for Bacillariophyta per sample, and the number of bacillariophyte peptides identified for ribosomal, photosynthetic, rubisco, flavodoxin and plastocyanin proteins in each sample.

Sample	All Bacillariophyta peptides (n)	Ribosomal peptides (n)	Photosynthetic peptides (n)	Rubisco peptides(n)	Flavodoxin peptides(n)	Plastocyanin peptides(n)
T0_A	341	37	26	8	4	4
T0_B	348	37	29	9	6	3
T0_C	421	55	37	9	7	2
in situ +Fe _A	1227	163	83	17	7	3
in situ +Fe _B	1351	179	93	19	11	3
in situ +Fe _C	1611	211	98	26	9	3
in situ _A	573	67	45	5	14	6
in situ _B	580	69	44	10	11	5
in situ _C	889	101	61	13	12	9
+4°C +Fe_A	1213	121	86	16	9	2
+4°C +Fe_B	1397	148	93	17	9	3
+4°C +Fe_C	1595	181	94	20	10	2
+4°C _A	552	60	35	10	11	4
+4°C _B	498	51	33	7	9	6
+4°C _C	764	67	47	9	13	7
Station 2_10m	105	18	7	1	2	1
Station2_25m	209	24	14	3	4	4
Station6_10m	693	108	44	10	10	5
Station6_30m	221	40	13	8	2	3
Station2_R_12m	318	41	27	10	5	2
Station2_R_25m	424	55	27	9	4	2

S7. The number of peptides identified for prymnesiophyceae per sample, and the number of prymnesiophyte peptides identified for ribosomal, photosynthetic, rubisco, flavodoxin and plastocyanin proteins in each sample.

Sample	All Prymnesiophyte Peptides (n)	Ribosomal Peptides (n)	Photosynthetic Peptides (n)	Rubisco Peptides (n)	Flavodoxin Peptides (n)	Plastocyanin Peptides (n)
T0_A	562	39	59	15	8	1
T0_B	601	52	78	20	8	1
T0_C	763	65	91	10	2	0
in situ +Fe _A	410	67	63	5	0	0
in situ +Fe _B	651	87	94	9	0	0
in situ +Fe _C	783	87	101	24	0	1
in situ _A	533	45	55	25	9	1
in situ _B	405	54	41	13	2	0
in situ _C	642	83	75	14	3	0
+4°C +Fe_A	298	34	61	5	2	0
+4°C +Fe_B	391	38	62	11	2	0
+4°C +Fe_C	643	85	96	9	2	0
+4°C _A	511	59	53	18	2	0
+4°C _B	489	42	51	19	2	0
+4°C _C	555	65	69	25	3	0
Station2_10m	397	51	33	6	2	0
Station2_25m	420	33	52	9	2	0
Station6_10m	266	52	18	4	1	0
Station6_30m	134	19	20	2	1	0
Station2_R_12m	321	39	43	7	2	0
Station2_R_25m	324	40	38	8	0	0